

**Analytical Solutions of the Minimal Nonlinear Equation for the Yaw
Response of Tail Fins and Wind Vanes.**

Mohamed M. Hammam

*Department of Mechanical Power Engineering,
Faculty of Engineering, Port Said University, Port Said, Egypt.**

David H. Wood

*Department of Mechanical and Manufacturing Engineering,
University of Calgary, 2500 University Dr., Calgary, Alberta T2N 1N4, Canada.*

(Dated: January 19, 2026)

Abstract

Analytical solutions for the yaw response of tail fins for small wind turbines, and wind vanes for wind direction measurement, are derived for any planform and any release angle γ_0 . This extends current linear models limited to small $|\gamma_0|$ and low aspect ratio planforms. The equation studied here is the minimal form of the general second order equation for the yaw angle, γ , derived by Hammam and Wood [1]. The nonlinear damping is controlled by a small parameter that depends on the vortex flow coefficient, K_v , which is absent from all linear models. The minimal equation is analysed using perturbation techniques. A truncated series solution from the Krylov-Bogoliubov-Mitropolskii averaging method compares favourably with a numerical solution apart from some small deviations at large time. Another form of averaging due to Beecham and Titchener [2] yields a compact solution in terms of the rate of amplitude decay, and the rate of change of phase angle. This allows the identification of an equivalent linear system with equivalent frequency and damping ratio. Two limiting analytic solutions for small and large $|\gamma_0|$ are obtained. The former is used to identify the model parameters from experimental data. Both approximate solutions showed that high K_v is important for fast decay of yaw amplitude for tail fins at high $|\gamma_0|$. High aspect ratios for wind vanes would reduce the nonlinearity to minimize yaw error. Linear response that is independent of K_v occurs whenever $\sin(\pi\gamma_0) \approx \pi\gamma_0$. Further, the low angle analytical solution allows an exact identification of the nonlinearity which could be used to extend the modelling of wind vanes to high γ .

I. INTRODUCTION

Many small horizontal-axis wind turbines use a tail fin to align the rotor with the wind, e.g. Wood [3] and Bradney *et al.* [4]. The unsteady aerodynamics of tail fins is very similar to that of wind vanes used to measure wind direction, e.g. Kristensen [5], Hristov *et al.* [6] and Kerhascoët *et al.* [7]. All these references used a second order, linear equation to describe unsteady yaw so the response can be characterized by the damping ratio and natural frequency which both depend on the fin or vane planform, e.g. Singh *et al.* [8] and Kerhascoët *et al.* [7]. In addition, the frequency is proportional to the wind speed, U , Khedr *et al.* [9]. The linear solution is limited to small magnitudes of the yaw angle, γ , and low aspect ratio, \mathcal{A} , defined as $\mathcal{A} = b_0^2/A$, where b_0 is the maximum span and A is the planform area.

* Contact author: m.hammam@eng.psu.edu.eg

The low- U behaviour of fins and vanes can be more complex and problematical than at higher speed. For example, the acceleration of the blades of a small turbine from rest at around 3 m/s, the typical “cut-in” wind speed for the commencement of power production, may involve large yaw angles and long starting times, Wood [3]. In addition, the frictional resistive torque in the bearings of fins and vanes may be significant at low wind speed. This paper describes work aimed at extending the yaw modelling to the nonlinear range to account for large yaw angles and to allow the modelling of friction. The theoretical extension is described by Hammam and Wood [1]. Khedr *et al.* [9] summarize the full nonlinear equations and compare their behaviour to wind tunnel experiments which include the “Test s” or TCs that will be the subject of our analysis. Model tail fins without a rotor or nacelle were mounted in a wind tunnel at an initial yaw angle, γ_0 , and released. Their subsequent oscillatory motion was recorded and the results compared to the theoretical predictions for a range of planforms, size, and \mathcal{R} . The lack of rotor and nacelle make the studies equally applicable to tail fins and wind vanes so that “fin” is here synonymous with “vane”. In nearly all these experiments, U was kept constant. The theory developed by Hammam and Wood [1] includes a term dependent on the rate of change of U but Khedr *et al.* [9] found that their wind tunnel did not allow a sufficiently rapid change in wind speed to test the extra term. Hence, we concentrate only on the behaviour for steady U .

Good agreement was found using model parameters established in prior numerical and experimental tests, and this was improved by the use of system identification of those parameters that were not known to high accuracy, Khedr *et al.* [10]. A simple analysis in Hammam and Wood [11] and the experiments of Khedr *et al.* [9] showed that nonlinearities in yaw response become important when γ_0 exceeds around 45° . One of our unexpected, new, and important findings in Sections IV and VIII A, however, is that nonlinearity persists down to very small yaw angles before becoming unimportant. Nevertheless, the full response equation is complicated and requires up to nine model constants, so Hammam and Wood [1] derived a reduced but still nonlinear, equation with fewer unknowns to replace the full equation in appropriate cases, but did not attempt to find its closed form solution. The subsequent work to develop an analytical solution is described herein. [10] found that the reduced model provided an accurate description of TC response if the model constants are optimized using system identification techniques. Therefore, we concentrate here on how those constants determine the solution so that fin and vane geometries can be better chosen to optimise the response.

There were several motivations for the present work, beginning with supporting the development

of a new tail fin module for the open-source aeroelastic code for wind turbines OpenFAST which can be downloaded from <https://www.nrel.gov/wind/nwtc/openfast.html>. Associated with this is the need to give better guidance for tail fin design, which currently relies more on rules-of-thumb and aesthetic considerations than on sound aerodynamic principles, Wood [3] and Bradney *et al.* [4]. Wind vane design is in a similar situation; Kerhascoët *et al.* [7] undertook a design optimization but this was limited by their restriction to linear behaviour. As yet, no detailed study has been made of the effects of power extraction by the rotor on the flow over the tail fin. The new OpenFAST module assumes a simple reduction in wind speed through the rotor. It is intended to test the validity of this assumption in wind tunnel and field tests of yawing small turbines. The effects of the rotor are ignored in this study.

The problem considered here is an example of a nonlinear damped oscillation which has an extensive literature, particularly for the case where the nonlinear terms are of second order. Then, the main emphasis is to determine whether the “damping” and “frequency” change, where the quotation marks emphasize that these quantities are a function of time, and possibly other variables, for a nonlinear system. The asymptotic expansion of nonlinear equations with a perturbation parameter, results in what is known as “secular” terms. These can make the solution aperiodic, or cause the response to grow in amplitude at large time. The secular terms result from truncation of the series expansion of the equations, to leave a finite number of terms and make the solution manageable, Mickens [12]. In order to eliminate the secular terms, the amplitude must be a function of time and the period a function of the amplitude as will be shown in the solution in Section III. These are basic features that differentiate between the response of linear and nonlinear systems.

Our aim is to find an approximate analytic solution to the nonlinear model developed by Hammam and Wood [1]. The specific aim is to derive the effective damping ratio and response frequency in terms of the geometric parameters of the tail fin to allow an assessment of their role in providing a desirable yaw alignment. The parameters include the length of the tail boom, x_p , and \mathcal{R} . Hammam and Wood [1] showed that high \mathcal{R} and large $|\gamma|$ are the main causes of nonlinearity with the latter causing the aerodynamic coefficients to become nonlinear in \mathcal{R} . Here we start with a simplified form of the model in which the “separation functions” that control the relative magnitude of the aerodynamic moments, are fixed. We call this the “minimal model” and the equation representing it the “minimal equation”. The impact of the separation functions on the current solution is discussed in Section IX.

The next section describes the dynamic response equation of Hammam and Wood [1] and the

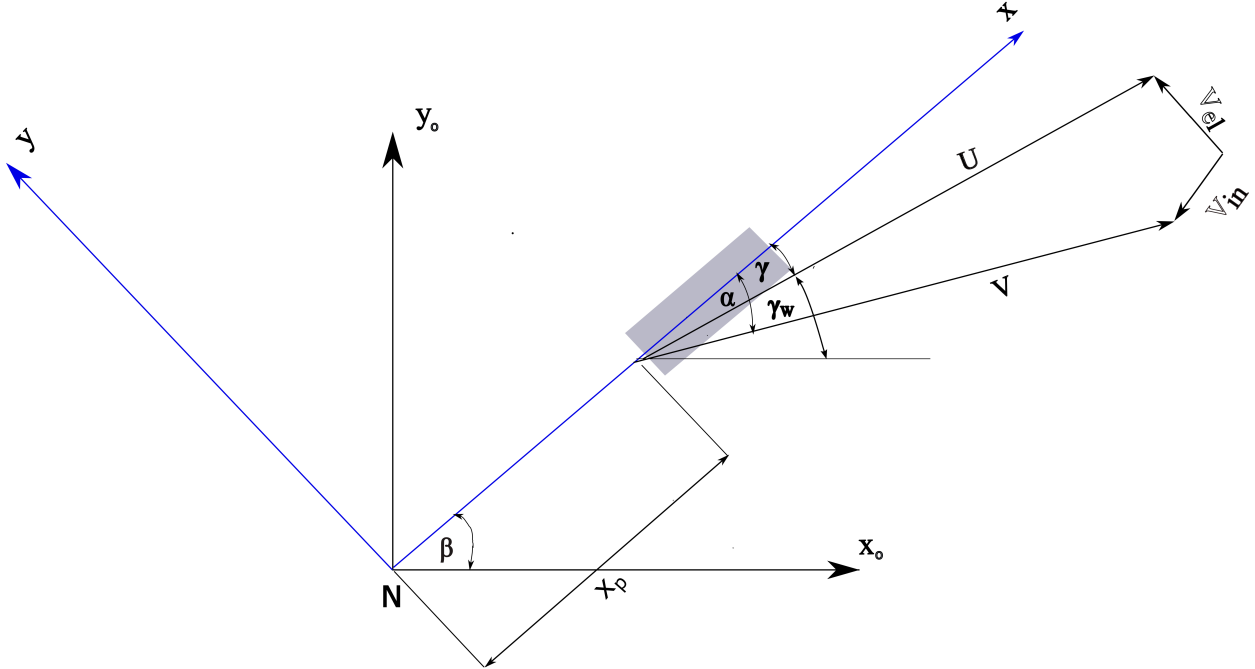


FIG. 1: Schematic plan view of tail fin motion and coordinate systems. The tail fin of exaggerated thickness is shaded. Figure taken from Hammam and Wood [1].

assumptions used to disregard high order terms. We present the equation in a standard form and make its parameters non-dimensional. The section ends with a discussion of the bounding linear solutions for $|\gamma| \rightarrow 0$ and $|\gamma| \rightarrow \pi/2$ which feature significantly in the subsequent analysis. Section III describes the use of the averaging method of Krylov and Bogoliubov [13] and Bogoliubov and Mitropolskii [14], the Krylov-Bogoliubov-Mitropolskii (KBM) method. Together with the series representation of the nonlinear term the result is a polynomial expression of the amplitude and phase in a form amenable for analytical solution. Identifying and quantifying the nonlinearity parameter and specifying the series truncation errors of the solution are the topics of Section IV. Section V describes the analytical solution and an analytical expressions for amplitude and phase are derived. Validation of the KBM solution by comparison to a numerical solution for the tail fin TCs is presented in Section VI. Section VII uses the more accurate Beecham and Titchener [2] (BT) averaging method, to provide a compact form of two important parameters that characterize the response: the decay and frequency. This leads to an equivalent linear system whose damping ratio and frequency are quantified. Analysis of the BT models in Section VIII includes a derivation for the two limiting cases of low and high $|\gamma_0|$. Section IX discusses the implications of simplifying the reduced model to the minimal form. Conclusions are given in Section X.

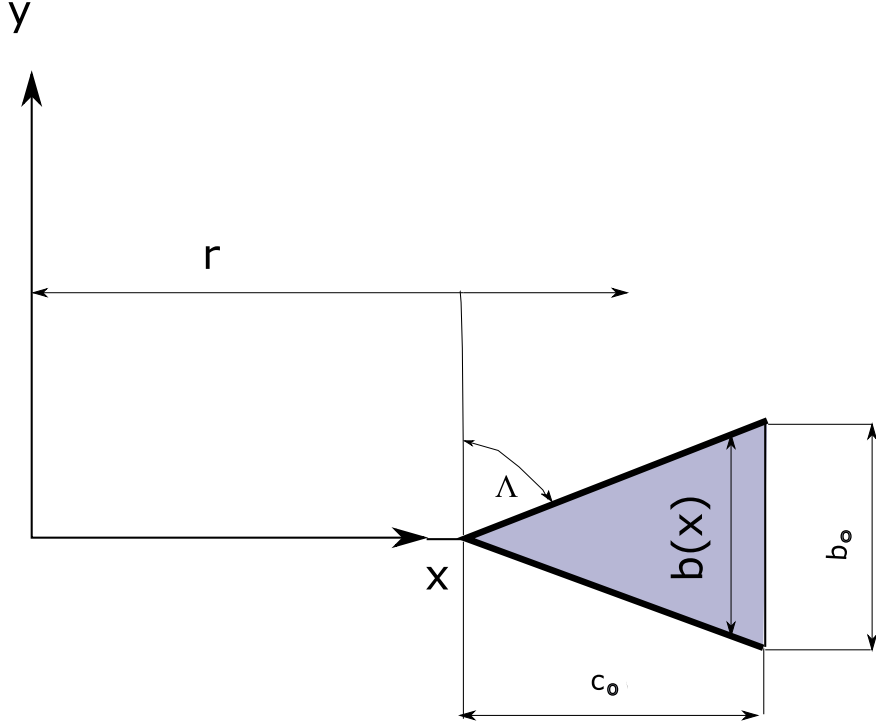


FIG. 2: Delta tail fin Schematic. Figure taken from Hammam and Wood [1].

II. THE NONLINEAR YAW RESPONSE EQUATION

Figure 1 is a plan view of a generic tail fin yawing about the inertial axis ($\mathbf{x}_0, \mathbf{y}_0$) fixed at \mathbf{N} with a tail boom of length x_p . For aeroelastic simulations of wind turbines, it is necessary to include the “induced” velocity, V_{in} , due to flow through the rotor, but $V_{in} = 0$ in the TCs. The “elastic” velocity V_{el} arises partly from any motion of the tower, which is absent in the TCs. V_{el} , however, includes the rotational velocity of the tail fin which depends on the rate of change of γ , $\dot{\gamma}$, and is normal to the tail fin surface. This velocity is the main difference between steady and unsteady yaw motion of tail fins and causes a difference between γ and α , the angle of attack in Fig. 1. All previous mathematical models of fins or vanes were derived either from thin airfoil theory, following Wieringa [15], or unsteady slender body theory (USBT), following Wood [3]. Both use a small angle approximation to obtain a linear, second order ordinary differential equation in γ by assuming that the vane rotational motion is slow compared to U , Jonsson [16]. For the TCs, however, α and γ are related by

$$\tan \alpha = \arctan \left(\tan \gamma + \frac{r \dot{\gamma}}{U \cos \gamma} \right) \approx \gamma + \frac{r \dot{\gamma}}{U}. \quad (1)$$

The use of α to determine the forces means that both theories mentioned above do not account properly for the suction force developed at the sharp and swept leading edge of the fin. This suction force tends to rotate the resultant force in the direction normal to the surface but not normal to the flow direction as assumed in the two theories, Robinson and Laurmann [17]. Hence the use of α for either resolving lift and drag in thin airfoil theory or for setting the boundary conditions in USBT is not correct and γ is the angle that gives the resultant normal force. The other fault of the linear theories is that both neglect the nonlinear dependence of the normal force on γ because they neglect the separation over all thin leading edges at high sweep angle, Λ as defined in Fig. 2. The flow tends to separate into two concentrated spiral vortices even at low angle creating an additional component of induced velocity and nonlinear dependency on γ . Many theories have been developed to model the effect of these vortices and supplement the basic linearized theory on highly swept surfaces. All of them failed to some extent due to the assumptions used to make the solution manageable, mainly that the flow is conical such that it can be considered two dimensional. Then, [18] formulated his leading edge suction analogy (LESA) which considered three dimensional flow and relaxed the assumption of small angle, Luckring [19]. The LESA was applied to model the tail fin response at high $|\gamma|$ by Ebert and Wood [20] and Singh *et al.* [8]. The reduced form of the high- $|\gamma|$ model is based mainly on the LESA with some modifications to account for the complex high angle separation of swept thin edge surfaces. as detailed in Hammam and Wood [1]. For analysing the TCs here, we limit γ_0 to $0 \leq |\gamma_0| \leq \pi/2$, as the limit angles admit the separate bounding linear solutions given in Subsection II C. The fin or vane is released from rest at γ_0 , giving two initial conditions, and the problem is to find the subsequent $\gamma(t)$, where t is time. A moment balance about N gives

$$I\ddot{\gamma} + M = 0 \quad (2)$$

where I is the fin or vane moment of inertia about the yaw axis including the tail boom inertia. M is the vane aerodynamic moment provided that friction can be ignored. The moment is taken from Eq. (13.1) of Hammam and Wood [1]:

$$\begin{aligned} I\ddot{\gamma} = & -0.5\rho Ar \left[x_1^* K_p (r\dot{\gamma} + U \sin \gamma) U \cos \gamma \right. \\ & \left. + (x_2^* K_v + (1 - x_3^*) C_{Dc}) (U \sin \gamma + r\dot{\gamma})^2 \operatorname{sign}(U \sin \gamma + r\dot{\gamma}) \right] \end{aligned} \quad (3)$$

where dots denote time derivatives and ρ is the air density. The main assumption behind this “reduced” equation is that $x_p \gg c_0$, where c_0 is the chord, defined in Fig. 2. This restriction makes the yaw response of vanes and fins different from, say, a delta wing pitching about its apex for which

$x_p = 0$. The large literature on pitching bodies is, therefore, not of direct relevance to our analysis. The LESA, unfortunately, does not give the load distributions but only the integrated force. Hammam and Wood [1] used USBT to derive the yaw moment, which gave lengthy integrals, dependent on the chordwise direction, that are planform dependent. As an alternative, we assumed the force obtained from LESA acts at the moment arm r , taken to be the distance from the vane geometric centre to the yaw axis as shown in Fig. 2, and the velocities are considered uniform over the fin or vane. These assumptions hold for most fins and vanes known to the authors and was tested for some of them in Khedr *et al.* [10]. The first term in the brackets contains the potential flow coefficient K_p , and the second term expresses vortex flow, bursting and, ultimately, flow separation at very high yaw angle. Subsection II C shows that these equations reduce to the linear form of Kristensen [5] which involves only K_p , so the main nonlinearities are associated with the vortex flow coefficient, K_v and C_{Dc} , the full separation drag coefficient. Values of K_p and K_v will be considered and used throughout this study and it is very important to note that (a) most were obtained from lift and drag measurements or calculations for steady flow, and (b) the unsteady values were obtained from system identification of wind tunnel results from model fins as described above. x_i^* for $i = 1, 2, 3$, are the separation functions. They express the contribution of each moment component as γ changes.

For brevity, we do not reproduce the derivation of Eq. (3) from Hammam and Wood [1]. The description in the last paragraph shows the major contribution of the LESA to the modelling of any planform; the reduction of the force acting on the these surfaces to coefficients which are planform and \mathcal{A} dependent extends the potential application of the model. This was done, for example, by Lamar [21] for a range of unusual planforms, and we note the success of the model for fins of complicated planforms by Khedr *et al.* [10].

A. The yaw response as a second order nonlinear equation

Equation (3) is now recast in a form suitable for solution using averaging methods. First, the different flow components are assumed to be always active over the tail fin surface, so $x_1^* = x_2^* = 1$. This implies that C_{Dc} will behave identically to K_v , so we set $x_3^* = 0$ and absorb the high- $|\gamma|$ drag into the vortex force coefficient. The reduced Eq. (3) now becomes the current “minimal equation”. In Section IX it will be shown that these x_i^* functions do affect the response and their modelling is important for accurate prediction of the experimental response. Our aim here, however, is to understand how the model coefficients affect the response and this can be done using the minimal

equation. Second, the moment of inertia is normalized to give the reduced moment of inertia defined by $I_* = 2I/(\rho AU^2r)$ which has dimensions of s^2 . Equation (3) becomes:

$$\ddot{\gamma} + \frac{1}{I_*} \left[\frac{r}{U} \cos \gamma \dot{\gamma} + \frac{1}{2} \sin 2\gamma \right] K_p + \frac{1}{I_*} \left[\sin \gamma + \frac{r \dot{\gamma}}{U} \right]^2 \operatorname{sign} \left[\sin \gamma + \frac{r \dot{\gamma}}{U} \right] K_v = 0. \quad (4)$$

Having two terms of different orders in the argument of the sign function makes it impossible to separate the terms containing γ from those depending on $\dot{\gamma}$.

1. Polynomial expansion of the trigonometric functions

In order to have Eq. (4) in standard form, the nonlinear trigonometric terms are transformed into polynomials. Using $\gamma^* = \gamma/\gamma_0$ as the normalized angle, the Chebyshev polynomials for $\sin(\cdot)$ and $\cos(\cdot)$ lead to

$$\cos(\gamma_0 \gamma^*) = J_0(\gamma_0) + 2 \sum_{k=1}^{\infty} (-1)^k J_{2k}(\gamma_0) T_{2k}(\gamma^*) \quad (5)$$

and

$$\sin(2\gamma_0 \gamma^*) = 2J_1(2\gamma_0)\gamma^* + 2 \sum_{k=1}^{\infty} (-1)^k J_{2k+1}(2\gamma_0) T_{2k+1}(\gamma^*) \quad (6)$$

Snyder [22]. $J_n(\cdot)$ is the Bessel function of the first kind of order n , and $T_k(\cdot)$ is the Chebyshev polynomial of order k . (The names, definitions, and symbols for all the special functions used herein are taken from Olver *et al.* [23] which will not be cited again.)

The expansion for sign term gives

$$\begin{aligned} & [\sin(\gamma_0 \gamma^*) + r_u \gamma_0 \dot{\gamma}^*]^2 \operatorname{sign} [\sin(\gamma_0 \gamma^*) + r_u \gamma_0 \dot{\gamma}^*] \\ &= \frac{8}{3\pi} [\sin(\gamma_0 \gamma^*) + r_u \gamma_0 \dot{\gamma}^*] - \frac{8}{\pi} \sum_{k=1}^{\infty} (-1)^k \frac{T_{2k+1}(\sin(\gamma_0 \gamma^*) + r_u \gamma_0 \dot{\gamma}^*)}{(4k^2 - 1)(2k + 3)} \end{aligned} \quad (7)$$

where $r_u = r/U$, as derived in Appendix A.

2. Series expansion of the yaw response

Substituting the trigonometric series expansions in Eqs. (5, 6, and 7) into Eq. (4) gives

$$\begin{aligned} \ddot{\gamma}^* &= -\frac{K_p}{I_* \gamma_0} \left[\sum_{k=0}^{\infty} (-1)^k J_{2k+1}(2\gamma_0) T_{2k+1}(\gamma^*) \right] - \frac{K_p r_u}{I_*} \left[\sum_{k=0}^{\infty} \epsilon_k (-1)^k J_{2k}(\gamma_0) T_{2k}(\gamma^*) \right] \dot{\gamma}^* \\ &\quad - \frac{K_v}{I_* \gamma_0} \left[\frac{8}{\pi} \sum_{k=0}^{\infty} (-1)^k \frac{T_{2k+1}(\sin(\gamma_0 \gamma^*) + r_u \gamma_0 \dot{\gamma}^*)}{(4k^2 - 1)(2k + 3)} \right]. \end{aligned} \quad (8)$$

where $\epsilon_k = 1$ for $k = 0$, and $\epsilon_k = 2$ for $k > 0$.

To simplify the solution without comprising the accuracy, the terms in the last series summation in Eq. (8) of $O(r_u^3\dot{\gamma}^3)$ and higher are disregarded. This is shown in Appendix B to result in the simplified form of the response equation that is presented in the following subsection.

B. Simplified response equation

If the second term in the Chebyshev polynomial argument of the last term of Eq. (8) is small, then Appendix B derives the approximate equation correct to $O(r_u^3\dot{\gamma}^3)$. Thus, Eq. (4) can be simplified to

$$\ddot{\gamma} + \frac{1}{I_*} \left[r_u \cos \gamma \dot{\gamma} + \frac{1}{2} \sin 2\gamma \right] K_p + \frac{1}{I_*} \left[\sin \gamma |\sin \gamma| + 2r_u \dot{\gamma} |\sin \gamma| + r_u^2 \dot{\gamma}^2 \operatorname{sign}[\gamma] \right] K_v = 0. \quad (9)$$

To check the accuracy of this approximation, Eq. (4) and Eq. (9) were solved numerically. All the numerical solutions presented herein were obtained using NDSolve in Mathematica without changing the default settings. A typical tail fin that is our TC1, is taken from Khedr *et al.* [9]. It has a delta planform with $c_0 = 0.27$ m and $b_0 = 0.078$ m, which gave $\mathcal{R} = 2b_0/c_0 = 0.58$, for which the force coefficients were $K_p = \pi \mathcal{R}/2 = 0.91$, and $K_v = \pi$. $r = 0.623$ m and I , the moment of inertia, was 0.047 kg m². The comparisons were done at the maximum $\gamma_0 = 90^\circ$ and $U = 17$ m/s, giving $I_* = 0.042$ s². Khedr *et al.* [9] showed that, for a fixed γ_0 , the experimental response scaled with U , so that $r_u \dot{\gamma}$ will depend only on γ_0 and is maximized when $\gamma_0 = \pi/2$.

The responses of the two equations are plotted in Fig. 3. Figure 4 shows that the maximum error of the third order approximation in r_u is around $\pm 0.81^\circ$, and the error decreases with time. The maximum value of $r_u \dot{\gamma}$ was 0.313. We conclude that Eq. (9) is sufficiently accurate to justify further analysis of it.

C. The bounding linear solutions and the onset of nonlinearity

In the limit as $|\gamma| \rightarrow 0$ with $r_u \dot{\gamma}$ remaining small, the leading terms in Eq. (9) are

$$\ddot{\gamma} + \frac{r_u K_p}{I_*} \dot{\gamma} + \frac{K_p}{I_*} \gamma = 0. \quad (10)$$

Thus, the yaw response is linearized and independent of γ_0 . As expected, Eq. (10) is also independent of the nonlinear factor K_v . The solution of Eq. (10) gives a damped oscillatory response with

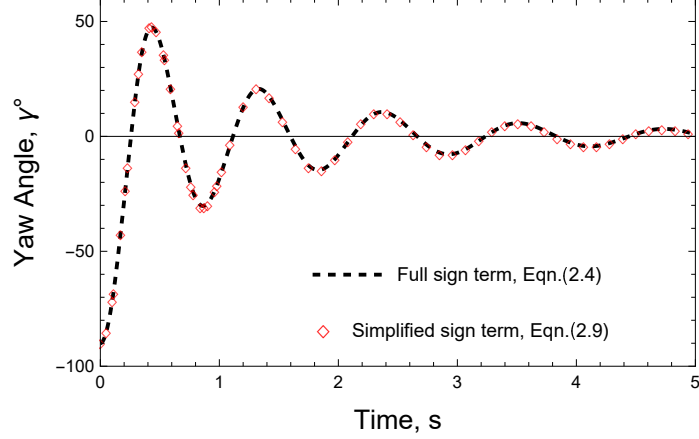


FIG. 3: Yaw response of TC1 tail fin at $U = 17$ m/s. Solution using Eq. (4) is shown in dashed black line, and using Eq. (9) in red diamond symbols.

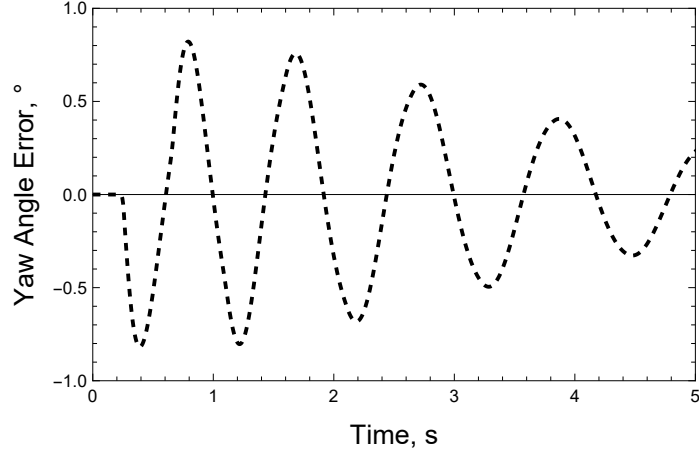


FIG. 4: Difference between the numerical solutions of Eqs. (4, 9) in figure 3.

a natural frequency, $\omega_{0,\text{lin}}$, of

$$\omega_{0,\text{lin}} = \sqrt{K_p/I_*} \quad (11)$$

and damping ratio, ζ_{lin} , of

$$\zeta_{\text{lin}} = \frac{r_u}{2} \sqrt{\frac{K_p}{I_*}} \propto r^{3/2} \sqrt{\frac{K_p A}{I}}. \quad (12)$$

and independent of U . These are Equations (40) and (41), respectively, for the frequency and damping for wind vanes in Kristensen [5] where his K is equivalent to K_p here.

For completeness, we include the well-known solution to Eq. (10):

$$\gamma = \gamma_0 \exp(-\zeta_{\text{lin}}\omega_{0,\text{lin}}t) \cos\left(\omega_{0,\text{lin}}\sqrt{1 - \zeta_{\text{lin}}^2}t\right). \quad (13)$$

The largest γ_0 we consider is $\pi/2$. With a change in variable to $\chi = \gamma_0 - \gamma$, Equation Eq. (9) becomes

$$\ddot{\chi} - \frac{K_p}{I_*} \chi - \frac{K_v}{I_*} = 0 \quad (14)$$

when $r_u \dot{\gamma}$ and χ are small, Khedr *et al.* [10]. In terms of γ , the solution is

$$\gamma = \gamma_0 - \frac{K_v}{K_p} \left[\cosh \left(\sqrt{\frac{K_p}{I_*}} t \right) - 1 \right] \sim \gamma_0 - \frac{K_v}{2I_*} t^2 - \frac{K_p K_v}{24I_*^2} t^4 - O \left(\frac{t^6}{I_*^3} \right) \quad (15)$$

and the response is clearly non-oscillatory which suggests that the nonlinearity quickly becomes important for high γ_0 .

The lowest order (nonlinear) terms that were omitted from the left hand side of Eq. (10) are

$$\frac{K_v}{I_*} \left(2r_u \gamma \dot{\gamma} + r_u^2 |\dot{\gamma}| \dot{\gamma} + \gamma^2 \right). \quad (16)$$

Classical methods for the solution of nonlinear oscillations, e.g. Mickens [12], require the nonlinear terms to be of the form $\epsilon F(\gamma, \dot{\gamma})$, where F denotes functional dependence and ϵ is a small perturbation parameter. Equation (9) is not of this form as it has two parameters, neither of which is generally small. Further, the perturbation parameter in general will be a function of γ_0 , but will be bounded by those in Eq. (16) as $\sin \gamma$ is always smaller in magnitude than γ .

As $\gamma_0 \rightarrow \pi/2$ the potential flow component diminishes and the K_p term can be set to zero. The lowest order terms omitted from Eq. (14) are

$$\frac{2r_u K_v}{I_*} \chi \dot{\chi} + \frac{r_u^2 K_v}{I_*} |\dot{\chi}| \dot{\chi} \quad (17)$$

based on the condition of $r_u \dot{\gamma} \ll 1$ which is valid at the start of the response. This reduces the solution in Eq. (15) to

$$\gamma \approx \gamma_0 - \frac{K_v}{2I_*} t^2 \quad (18)$$

which accurately reproduces the initial response of a rectangular fin at high $|\gamma_0|$ in figure 3 of Khedr *et al.* [10]. As expected, the high $|\gamma_0|$ response is dominated initially by K_v .

D. The response equation in nondimensional form

There are two possible parameters which would nondimensionalize the time, t ; $\sqrt{I_*}$ or r_u . We chose to transform t to $t_* = t/\sqrt{I_*}$ as suggested by Eq. (18). This makes the coefficient of $d^2 \gamma / dt_*^2$

TABLE I: The main parameters of the minimal equation. I_* and r_u have dimensions s^2 and s respectively. The remaining parameters have no dimensions.

| | | | | | | |
|-------------------------|-------------|-------------------|--------------------------|----------------------------------|---------------|------------------------------|
| $I_* = 2I/(\rho AU^2r)$ | $r_u = r/U$ | $\beta = K_v/K_p$ | $\beta_1 = K_p/\gamma_0$ | $\beta_2 = K_p r_u / \sqrt{I_*}$ | $t_* = t/I_*$ | $\gamma^* = \gamma/\gamma_0$ |
|-------------------------|-------------|-------------------|--------------------------|----------------------------------|---------------|------------------------------|

equal to unity. As stated previously, γ is nondimensionalised by γ_0 to give $\gamma^* = \gamma/\gamma_0$. Equation (9) becomes

$$\ddot{\gamma}^* + \frac{\beta_1}{2} \sin(2\gamma_0\gamma^*) + \beta_2 \cos(\gamma_0\gamma^*) \dot{\gamma}^* + \beta\beta_1 \left[\left(\sin(\gamma_0\gamma^*)^2 + \frac{2\beta_2\dot{\gamma}^*}{\beta_1} \right) \text{sign}[\sin(\gamma_0\gamma^*)] + \left(\frac{\beta_2\dot{\gamma}^*}{\beta_1} \right)^2 \text{sign}[\gamma_0\gamma^*] \right] = 0. \quad (19)$$

where $\beta = K_v/K_p$, $\beta_1 = K_p/\gamma_0$, and $\beta_2 = K_p r_u / \sqrt{I_*}$ are the parameters that will be investigated in the Section 6. Because these parameters appear throughout the remaining text, they are given for ease of reference in Table I. The initial conditions are $\gamma^*(t = 0) = 1$ and $\dot{\gamma}^*(t = 0) = 0$. To standardize the response equation, damping and natural frequency terms with coefficients 2σ and ν^2 , respectively, are added to the left side of Eq. (19) and equivalent terms with coefficients $\epsilon\sigma^*$, and $\epsilon\omega^{*2}$ are added to the right side to give

$$\ddot{\gamma}^* + 2\sigma\dot{\gamma}^* + \nu^2\gamma^* = \epsilon F(\gamma^*, \dot{\gamma}^*). \quad (20)$$

where σ , ν , are the equivalent linear damping and frequency to be found during the solution process. The nonlinear right hand side $\epsilon F(\gamma^*, \dot{\gamma}^*)$ is a function of the perturbation parameter, ϵ which will be determined in Section IV and shown to be a linear function of β_2 . Thus, the the last term in the last bracket of Eq. (19) is of second order and can be neglected. $\epsilon F(\gamma^*, \dot{\gamma}^*)$ is given by

$$\epsilon F(\gamma^*, \dot{\gamma}^*) = -\frac{\beta_1}{2} \sin(2\gamma_0\gamma^*) - \beta_2 \cos(\gamma_0\gamma^*) \dot{\gamma}^* - \beta\beta_1 \left(\sin(\gamma_0\gamma^*) + \frac{2\beta_2\dot{\gamma}^*}{\beta_1} \right) |\sin(\gamma_0\gamma^*)| + \sigma^* \dot{\gamma}^* + \omega^{*2} \gamma^*. \quad (21)$$

III. SOLUTION OF THE YAW RESPONSE EQUATION

Perturbation methods are powerful techniques for obtaining approximate closed form solutions to nonlinear second order differential equations of the forms studied here. Three basic perturbation

methods are most commonly used, namely: the Lindstedt-Poincare method, the averaging methods, and the the method of multiple scales, Mickens [12]. Of these, the KBM method, due to Krylov and Bogoliubov [13] and Bogoliubov and Mitropolskii [14], is the most suitable for the present analysis. A major advantage of averaging is that it transforms the complicated second nonlinear equation into two separable first-order equations which are straightforward to solve. In contrast, the multiple scale method leads to partial differential equations which can get complicated for complex nonlinear equations. A further advantage of the averaging method is that the solution is not determined by the need to get higher orders of the series expansion, but by ensuring the asymptotic behaviour as the perturbation parameter $\epsilon \rightarrow 0$ for each term of the series. This makes the determination of the higher order terms of the series independent of the higher harmonics in contrast to the Lindstedt-Poincare method.

In this section, we describe the application of the KBM method of averaging for the undamped system, as detailed in the Appendix C, and as extended by Mendelson [24] for finite damping.

Following the KBM method, we seek a solution that reduces to its linear equivalent in the limit $\epsilon F(\gamma^*, \dot{\gamma}^*) \rightarrow 0$. The solution has the form

$$\gamma^* = \gamma^*(a, \psi) = \gamma_0^* + \epsilon \gamma_1^* + \epsilon^2 \gamma_2^* \quad (22)$$

where a is the amplitude and ψ is the phase angle of period 2π . Note that the subscript “0” indicates the linear solution for γ^* in the limit $\epsilon \rightarrow 0$, and not the initial condition on γ . The first order approximation to Equation Eq. (22) is

$$\gamma^* = \gamma_0^* = a \cos \psi. \quad (23)$$

For the linear solution of Eq. (13), $a = \exp(-\zeta_{\text{lin}} \omega_{0,\text{lin}} t)$ and $\psi = \omega_{0,\text{lin}} (1 - \zeta_{\text{lin}}^2)^{1/2} t$. The frequency, $\omega = d\psi/dt = \omega_{0,\text{lin}} (1 - \zeta_{\text{lin}}^2)^{1/2}$. The relation $\omega = d\psi/dt$ holds for all linear and nonlinear systems. To first order in the perturbation parameter ϵ , a and ψ are given by first order differential equations:

$$\frac{da}{dt} = -\sigma a + \epsilon \zeta_1(a). \quad (24)$$

and

$$\frac{d\psi}{dt} = \omega_0 + \epsilon \omega_1(a) \quad (25)$$

such that $\omega_0 = \sqrt{\nu^2 - \sigma^2}$. The following assumption is used in the KBM method, Mickens [12]:

$$\zeta_1(a) \cos \psi - a \omega_1(a) \sin \psi = 0. \quad (26)$$

This restriction is necessary for simplifying $\dot{\gamma}^*$ to

$$\dot{\gamma}^* = -(\sigma \cos \psi + \omega_0 \sin \psi)a. \quad (27)$$

The consequences of this assumption and its impact on the accuracy of the solution will be assessed in Section VII.

The unknown functions $\zeta_1(a)$ and $\omega_1(a)$ are determined from the condition that Eq. (22) satisfies Eq. (20) for each order of ϵ . The leading terms in Eq. (24) and Eq. (25) are chosen such that the linear solution is recovered as $\epsilon F(\gamma^*, \dot{\gamma}^*) \rightarrow 0$. The resulting systems of second order equations in $\zeta(a)$ and $\omega(a)$ can be solved by expressing these variables as a power series in a :

$$\zeta_1(a) = \sum_{k=2}^{2m+1} A_k^{(1)} a^k \quad (28)$$

and

$$\omega_1(a) = \sum_{k=2}^{2m+1} B_k^{(1)} a^{k-1} \quad (29)$$

where m depends on the degree of the truncated terms of the series. For most systems, the first order solution given by Eq. (23) and in Eqs. (24,25) are sufficient to represent the approximate solution of Eq. (22), Bojadziev [25]. We also confirmed that the higher order terms were negligible. This occurs generally when the nonlinear function in Eq. (20) contains terms of odd degrees which is indeed the case for Eq. (19).

The coefficients A_k and B_k are obtained from the requirement that the secular terms vanish for any value of σ , see Appendix C. Upon substituting Eqs. (23, 28, and 29) into Eq. (19) and expanding $\epsilon F(\gamma^*, \dot{\gamma}^*)$ in Eq. (20) as a Fourier series of γ^* to give

$$2\omega_0\omega_1 a + \sigma a \frac{d\zeta_1}{da} - \sigma \zeta_1 = -F_1(a) \quad (30)$$

and

$$2\omega_0\zeta_1 - \sigma a^2 \frac{d\omega_1}{da} = -G_1(a) \quad (31)$$

where $F_1(a)$ and $G_1(a)$ are, respectively, the even and odd first coefficients of the Fourier series expansion of $\epsilon F(\gamma^*, \dot{\gamma}^*)$ given as

$$F(a \cos \psi, -\omega_0 a \sin \psi - \sigma a \cos \psi) = \frac{F_0(a)}{2} + \sum_{n=1}^{\infty} [F_n(a) \cos n\psi + G_n(a) \sin n\psi]. \quad (32)$$

The coefficients $F_n(a)$, $G_n(a)$ can be expanded in a series in the amplitude a as:

$$F_n(a) = \sum_{k=1}^{2m+1} F_k^{(n)} a^k, \text{ and} \quad (33)$$

$$G_n(a) = \sum_{k=1}^{2m+1} G_k^{(n)} a^k. \quad (34)$$

Substituting Eqs. (28 and 29) into Eqs. (30 and 31) and retaining the first harmonics ($n = 1$) of Eq. (32) results in the following equations for the coefficients of ζ_1 and ω_1 :

$$A_k^{(1)} = -\frac{(k-1)\sigma F_k^{(1)} + 2\omega_0 G_k^{(1)}}{4\omega_0^2 + (k-1)^2\sigma^2} \quad (35)$$

and

$$B_k^{(1)} = -\frac{2\omega_0 F_k^{(1)} - (k-1)\sigma G_k^{(1)}}{4\omega_0^2 + (k-1)^2\sigma^2}. \quad (36)$$

Substituting Eqs. (35 and 36) into (28 and 29) allows the solution of Eqs. (24 and 25).

A. Application of the averaging method to the yaw response equation

In order to solve Eqs. (24 and 25) analytically, the value of $m = 2$ is used. This makes the RHS of Eq. (24) a quintic polynomial in a . Equations (24 and 25) are

$$\frac{da}{dt} = -\sigma a + \epsilon A_3^{(1)} a^3 + \epsilon A_5^{(1)} a^5 \quad (37)$$

and

$$\frac{d\psi}{dt} = \omega_0 + \epsilon B_3^{(1)} a^2 + \epsilon B_5^{(1)} a^4. \quad (38)$$

The Fourier coefficients for $n = 1$, $F_i^{(1)}$ and $G_i^{(1)}$ of $F(\gamma^*, \dot{\gamma}^*)$ as expressed by Eq. (32) were calculated as

$$F_1(a) = \frac{1}{\pi} \int_0^{2\pi} F(a \cos \psi, -\omega_0 a \sin \psi - \sigma a \cos \psi) \cos \psi d\psi = F_1^{(1)} a + F_3^{(1)} a^3 + F_5^{(1)} a^5 \quad (39)$$

and

$$G_1(a) = \frac{1}{\pi} \int_0^{2\pi} G(a \cos \psi, -\omega_0 a \sin \psi - \sigma a \cos \psi) \sin \psi d\psi = G_1^{(1)} a + G_3^{(1)} a^3 + G_5^{(1)} a^5 \quad (40)$$

where all the even coefficients vanish. The coefficients $F_1(a)$ and $G_1(a)$ are obtained by integrating the nonlinear function from Eq. (21) using Mathematica as

$$\begin{aligned} F_1(a) = & -\beta_1 J_1(2\gamma_0 a) + \frac{2\beta_2 \sin \phi}{\gamma_0} (J_1(\gamma_0 a) - a\gamma_0 J_2(\gamma_0 a)) \\ & -\beta\beta_1 \text{sign}(\gamma_0) \left[H_1(2a\gamma_0) + \frac{4\beta_2 \sin \phi (a\gamma_0 H_0(a\gamma_0) - H_1(a\gamma_0))}{\beta_1 \gamma_0} \right] \\ & -(\sigma^* \sin \phi - \omega^{*2})a \end{aligned} \quad (41)$$

and

$$G_1(a) = \frac{2\beta_2 \cos \phi}{\gamma_0} J_1(\gamma_0 a) + \beta \beta_2 \operatorname{sign}(\gamma_0) \left[\frac{4\mathbf{H}_1(a\gamma_0) \cos \phi}{\gamma_0} \right] - \sigma^* a \cos \phi \quad (42)$$

where $\mathbf{H}_0(\cdot)$ and $\mathbf{H}_1(\cdot)$ are Struve functions. The terms in the first and the second lines result from integrating the respective terms in Eq. (21). In deriving the equations, the yaw rate from Eq. (27) is set to the form $\dot{\gamma}^* = -\sin(\psi + \phi)a$, such that $\sin \phi = \sigma$, and $\cos \phi = \omega_0$. As $\sin \phi \approx O(\beta_2)$, the second term in the brackets of Eq. (41) is of the order $O(\beta_2^2)$ and is negligible as found before. This results in a simpler expressions of the Fourier coefficients as

$$F_1(a) = -\beta_1 [J_1(2\gamma_0 a) + \beta \operatorname{sign}(\gamma_0) \mathbf{H}_1(2a\gamma_0)] + \omega^{*2} a \quad (43)$$

and

$$G_1(a) = \frac{2\beta_2 \cos \phi}{\gamma_0} [J_1(\gamma_0 a) + 2\beta \operatorname{sign}(\gamma_0) \mathbf{H}_1(a\gamma_0)] - \sigma^* a \cos \phi \quad (44)$$

B. Analytical representation of the response equation

KBM requires the Fourier coefficients of the nonlinear function to be in a polynomial form. The functions $F_1(a)$ and $G_1(a)$ can be approximated as polynomials in the amplitude allowing analytical solution using approximate methods, Beléndez *et al.* [26]. As the argument spans $a \in [0, 1]$, we used Chebyshev polynomials of the first kind, $T_{2n+1}(a)$. The approximation is most accurate over the interval $\pi/4 < |\gamma| < \pi/2$, Teron *et al.* [27], which makes it immediately suitable for high $|\gamma|$.

In order to get the F_1 and G_1 functions in a polynomial of a , the Bessel functions are expanded in a Chebyshev series of a as

$$J_{2k+1}(\gamma_0 a) = 2 \sum_{n=0}^m J_{k+n+1}(\gamma_0/2) J_{k-n}(\gamma_0/2) T_{2n+1}(a). \quad (45)$$

The Struve function expansion in terms of Chebyshev series is derived from the Schlömilch series of non alternating sign stated in Actor [28, Section 3.B] as

$$\mathbf{H}_1(a\gamma_0) = \frac{2\gamma_0^2}{3\pi} \sum_{n=0}^m \frac{{}_2F_3\left(2, 1; 5/2, n + 5/2, 3/2 - n; -\gamma_0^2/4\right)}{\Gamma(3/2 - n) \Gamma(n + 5/2)} T_{2n+1}(a) \quad (46)$$

where ${}_2F_3$ is the generalized hypergeometric function, and $\Gamma(\cdot)$ is the Gamma function. To express the Fourier coefficients as a polynomial in a , the odd Chebyshev polynomial T_{2n+1} is expressed in

terms of the hypergeometric function ${}_2F_1$, Luke [29, Eq. (9), Sec.8.5.1]:

$$T_{2n+1}(a) = (-1)^n (2n+1) a {}_2F_1 \left(-n, n+1; 3/2; a^2 \right). \quad (47)$$

${}_2F_1$ has a terminating series if either the first or the second arguments are non positive integers which gives

$$T_{2n+1}(a) = (-1)^n (2n+1) a \sum_{k=0}^n \frac{(-1)^k \Gamma(k+n+1)}{\Gamma(2k+2) \Gamma(-k+n+1)} (2a)^{2k}. \quad (48)$$

Similarly to the Struve function in Eq. (46), the Bessel function in Eq. (45) is expressed in terms of ${}_2F_3$, using the identity of Bessel functions products from Luke [29, Eq. (39), Sec.6.2.7] and replacing them in Eq. (45) to give

$$J_1(a\gamma_0) = \left(\frac{\gamma_0}{2}\right) \sum_{n=0}^m \frac{(-1)^n {}_2F_3 \left(1+n, 3/2+n; n+2, n+1, 2n+2; -\gamma_0^2/4 \right)}{\Gamma(n+2) \Gamma(n+1)} \left(\frac{\gamma_0}{4}\right)^{2n} T_{2n+1}(a). \quad (49)$$

To the authors' knowledge, the series representations of the \mathbf{H} and J functions of the first kind in Eqs. (46 and 49) respectively are derived herein for the first time. They are valid only for $a \geq 0$. Substituting Eqs. (46, 48, and 49) in (43 and 44) gives $F_1(a)$ and $G_1(a)$ as

$$\begin{aligned} F_1(a) = & -a\beta_1 \sum_{n=0}^m (2n+1) \left[2\Gamma(2n+2) {}_2\tilde{F}_3 \left(1+n, 3/2+n; n+2, n+1, 2n+2; -\gamma_0^2 \right) \right. \\ & \times \left(\frac{\gamma_0}{2} \right)^{2n+1} + \frac{2\beta|\gamma_0|}{\sqrt{\pi}} (-1)^n {}_2\tilde{F}_3 \left(2, 1; 5/2, n+5/2, 3/2-n; -\gamma_0^2 \right) \left. \right] \\ & \times \sum_{k=0}^n \frac{(-1)^k \Gamma(k+n+1)}{\Gamma(2k+2) \Gamma(-k+n+1)} (2a)^{2k} + \omega^{*2} a \end{aligned} \quad (50)$$

and

$$\begin{aligned} G_1(a) = & a\beta_2 \cos \phi \sum_{n=0}^m (2n+1) \left[\Gamma(2n+2) \right. \\ & \times {}_2\tilde{F}_3 \left(1+n, 3/2+n; n+2, n+1, 2n+2; -\gamma_0^2/4 \right) \left(\frac{\gamma_0}{4} \right)^{2n} + \frac{2\beta|\gamma_0|}{\sqrt{\pi}} (-1)^n \\ & \times {}_2\tilde{F}_3 \left(2, 1; 5/2, n+5/2, 3/2-n; -\gamma_0^2/4 \right) \left. \right] \sum_{k=0}^n \frac{(-1)^k \Gamma(k+n+1)}{\Gamma(2k+2) \Gamma(-k+n+1)} (2a)^{2k} \\ & - \sigma^* a \cos \phi \end{aligned} \quad (51)$$

where ${}_2\tilde{F}_3(a_1, a_2; b_1, b_2, b_3; z) = {}_2F_3(a_1, a_2; b_1, b_2, b_3; z) / \Gamma(b_1)/\Gamma(b_2)/\Gamma(b_3)$ is the “regularized” ${}_2F_3$, Straton [30]. These formulations of the Fourier coefficients allow their straightforward expression in ascending order of a . To approximate F_1 and G_1 as fifth order polynomials in a , $m = 2$ is set in Eqs. (50 and 51). Also, the power series coefficients of a , $F_{2k+1}^{(1)}$ and $G_{2k+1}^{(1)}$ in Eq. (34) are easily obtained by setting $k = 0, 1, 2$ in Eqs. (50, 51). When $k = 0$, the coefficients of a are

$$\begin{aligned} F_1^{(1)} &= -\beta_1 \sum_{n=0}^m (2n+1) \left[2\Gamma(2n+2) {}_2\tilde{F}_3\left(1+n, 3/2+n; n+2, n+1, 2n+2; -\gamma_0^2\right) \right. \\ &\quad \left. \times \left(\frac{\gamma_0}{2}\right)^{2n+1} + \frac{2\beta|\gamma_0|\gamma_0}{\sqrt{\pi}} (-1)^n {}_2\tilde{F}_3\left(2, 1; 5/2, n+5/2, 3/2-n; -\gamma_0^2\right) \right] + \omega^{*2}, \text{ and} \\ G_1^{(1)} &= \beta_2 \cos \phi \sum_{n=0}^m (2n+1) \left[\Gamma(2n+2) {}_2\tilde{F}_3\left(1+n, 3/2+n; n+2, n+1, 2n+2; -\gamma_0^2/4\right) \right. \\ &\quad \left. \times \left(\frac{\gamma_0}{4}\right)^{2n} + \frac{2\beta|\gamma_0|}{\sqrt{\pi}} (-1)^n {}_2\tilde{F}_3\left(2, 1; 5/2, n+5/2, 3/2-n; -\gamma_0^2/4\right) \right] \\ &\quad - \sigma^* \cos \phi \end{aligned} \quad (52)$$

Setting $F_1^{(1)} = 0$ and $G_1^{(1)} = 0$, the equivalent linear damping and frequency in Eq. (20) are obtained as

$$\begin{aligned} \sigma &= \frac{\sigma^*}{2} \\ &= \frac{\beta_2}{2} \sum_{n=0}^m (2n+1) \left[\Gamma(2n+2) {}_2\tilde{F}_3\left(1+n, 3/2+n; n+2, n+1, 2n+2; -\gamma_0^2/4\right) \left(\frac{\gamma_0}{4}\right)^{2n} \right. \\ &\quad \left. + \frac{2\beta|\gamma_0|}{\sqrt{\pi}} (-1)^n {}_2\tilde{F}_3\left(2, 1; 5/2, n+5/2, 3/2-n; -\gamma_0^2/4\right) \right] \end{aligned} \quad (53)$$

and

$$\begin{aligned} \nu^2 &= \omega^{*2} \\ &= \beta_1 \sum_{n=0}^m (2n+1) \left[2\Gamma(2n+2) {}_2\tilde{F}_3\left(1+n, 3/2+n; n+2, n+1, 2n+2; -\gamma_0^2\right) \left(\frac{\gamma_0}{2}\right)^{2n+1} \right. \\ &\quad \left. + \frac{2\beta|\gamma_0|\gamma_0}{\sqrt{\pi}} (-1)^n {}_2\tilde{F}_3\left(2, 1; 5/2, n+5/2, 3/2-n; -\gamma_0^2\right) \right]. \end{aligned} \quad (54)$$

The remaining coefficients are

$$\begin{aligned}
F_3^{(1)} &= \frac{2\beta_1}{3} \sum_{n=1}^m n(n+1)(2n+1) \left[2\Gamma(2n+2) {}_2F_3 \left(1+n, 3/2+n; n+2, n+1, 2n+2; -\gamma_0^2 \right) \right. \\
&\quad \left. \times \left(\frac{\gamma_0}{2} \right)^{2n+1} + \frac{2\beta|\gamma_0|\gamma_0}{\sqrt{\pi}} (-1)^n {}_2F_3 \left(2, 1; 5/2, n+5/2, 3/2-n; -\gamma_0^2 \right) \right], \\
F_5^{(1)} &= 16\beta_1 \left[\frac{64\beta\gamma_0|\gamma_0| {}_2F_3 \left(1, 2; -1/2, 5/2, 9/2; -\gamma_0^2 \right)}{315\pi^2} - \frac{\gamma_0^5}{192} {}_1F_2 \left(7/2; 4, 6; -\gamma_0^2 \right) \right], \\
G_3^{(1)} &= \frac{-2\beta_2 \cos \phi}{3} \sum_{n=1}^m n(n+1)(2n+1) \left[\Gamma(2n+2) \right. \\
&\quad \times {}_2F_3 \left(1+n, 3/2+n; n+2, n+1, 2n+2; -\gamma_0^2/4 \right) \left(\frac{\gamma_0}{4} \right)^{2n} \\
&\quad \left. + \frac{2\beta|\gamma_0|}{\sqrt{\pi}} (-1)^n {}_2F_3 \left(2, 1; 5/2, n+5/2, 3/2-n; -\gamma_0^2/4 \right) \right], \text{ and} \\
G_5^{(1)} &= 16\beta_2 \cos \phi \left[\frac{\gamma_0^4 {}_1F_2 \left(7/2; 4, 6; -\frac{\gamma_0^2}{4} \right)}{3072} - \frac{64\beta|\gamma_0| {}_2F_3 \left(1, 2; -1/2, 5/2, 9/2; -\frac{\gamma_0^2}{4} \right)}{315\pi^2} \right].
\end{aligned} \tag{55}$$

IV. NONLINEAR PERTURBATION PARAMETER AND ERROR ANALYSIS

In this section, an expression of the perturbation parameter ϵ is developed and an estimation of the error resulting from truncating the series of the coefficients Eq. (50) and (51) are stated.

The terms in the nonlinear function $\epsilon F(\gamma^*, \dot{\gamma}^*)$ from Eq. (21) are expressed as Chebyshev series to separate the γ^* terms using the expansions in Eqs. (5 and 6). We use the following series expansions for the sin terms:

$$|\sin(\gamma_0\gamma^*)| = - \left[E_0(\gamma_0) + 2 \sum_{k=1}^{\infty} (-1)^k E_{2k}(\gamma_0) T_{2k}(\gamma^*) \right] \tag{56}$$

$$\begin{aligned}
|\sin(\gamma_0\gamma^*)| \sin(\gamma_0\gamma^*) &= \left(\frac{2}{\pi} - E_1(2\gamma_0) \right) \gamma^* \\
&\quad + \sum_{k=1}^{\infty} (-1)^k \left(\frac{2}{\pi(2k+1)} - E_{2k+1}(2\gamma_0) \right) T_{2k+1}(\gamma^*)
\end{aligned} \tag{57}$$

where $E_k(\cdot)$ are Weber functions of order k as derived in Appendix D. The series expansion for T_{2k+1} is given by Eq. (48) and for T_{2k} by

$$T_{2k}(\gamma^*) = (-1)^k + (-1)^k k \sum_{n=1}^k \frac{(-4)^n \Gamma(k+n)}{\Gamma(2n+1) \Gamma(-n+k+1)} (\gamma^*)^{2n} \tag{58}$$

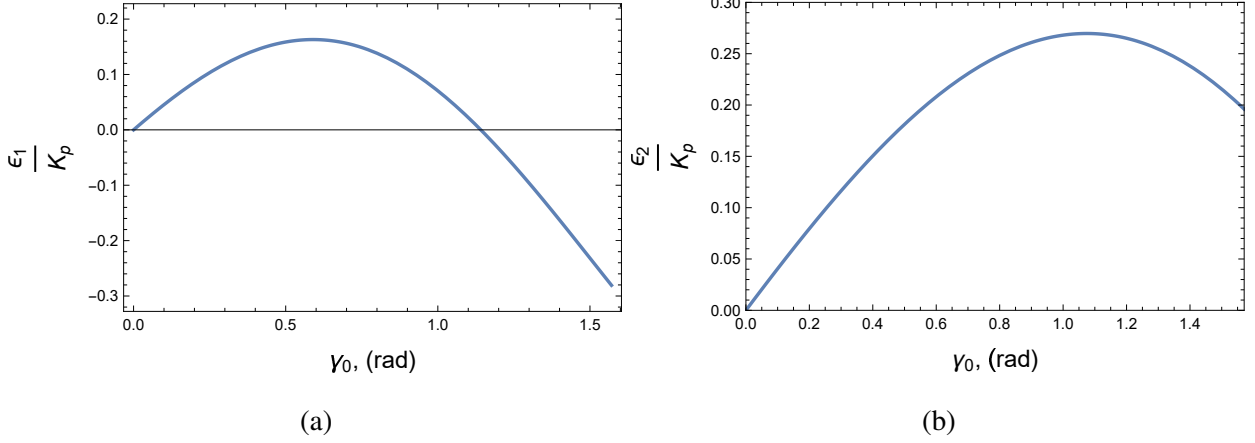


FIG. 5: Variation of the perturbation parameters change with γ_0 for TC1 described at the beginning of subsection II B. a) ϵ_1/K_p , b) ϵ_2/K_p .

are substituted above to separate $\epsilon F(\gamma^*, \dot{\gamma}^*)$ into nonlinear, $\epsilon F(\gamma^*, \dot{\gamma}^*)_{nl}$, and linear terms.

$$\begin{aligned} \epsilon F(\gamma^*, \dot{\gamma}^*)_{nl} &= \beta_1 \sum_{k=1}^{\infty} (-1)^k \left[J_{2k+1}(2\gamma_0) + \beta \left(\frac{2}{\pi(2k+1)} - E_{2k+1}(2\gamma_0) \right) \right] S_1 \\ &\quad + 2\beta_2 \sum_{k=1}^{\infty} (-1)^k [J_{2k}(\gamma_0) - 2\beta E_{2k}(\gamma_0)] S_2. \end{aligned} \quad (59)$$

where S_1 and S_2 , the series summation of γ^* from Eqs. (48 and 58), are given respectively as

$$\begin{aligned} S_1 &= (-1)^k (2k+1) \sum_{n=1}^k \frac{(-4)^n \Gamma(k+n+1)}{\Gamma(2n+2) \Gamma(-n+k+1)} (\gamma^*)^{2n+1} \\ S_2 &= (-1)^k k \sum_{n=1}^k \frac{(-4)^n \Gamma(k+n)}{\Gamma(2n+1) \Gamma(-n+k+1)} (\gamma^*)^{2n} \dot{\gamma}^* \end{aligned} \quad (60)$$

and the linear terms are $K_p \gamma^* + \beta_2 \dot{\gamma}^*$ which are the (linear) terms of Eq. (10). The series in Eq. (59) can be summed to give $\epsilon F(\gamma^*, \dot{\gamma}^*)_{nl} = F(\epsilon_1 \gamma^*, \epsilon_2 \dot{\gamma}^*)_{nl}$ in terms of two separate parameters as

$$\begin{aligned} \epsilon_1 &= \beta_1 [\sin(\gamma_0) (\cos(\gamma_0) + \beta \sin(\gamma_0)) - (J_1(2\gamma_0) + \beta H_1(2\gamma_0))], \text{ and} \\ \epsilon_2 &= \beta_2 [(\cos(\gamma_0) + 2\beta \sin(\gamma_0)) - (J_0(\gamma_0) + 2\beta H_0(\gamma_0))]. \end{aligned} \quad (61)$$

To the authors' knowledge, the series summations of Weber functions in Eq. (59) are stated here for the first time. Figure 5 shows ϵ_1/K_p , part (a), and ϵ_2/K_p , part (b), for TC1. Both are less than unity throughout the range of γ_0 . The perturbation is independent of U while it increases with β and \sqrt{r} . For small γ_0 the perturbation parameters are independent of K_p and are linear in γ_0 :

$$\epsilon_1 = K_v \left(1 - \frac{8}{3\pi} \right) \gamma_0 \text{ and } \epsilon_2 = \frac{2K_v r_u}{\sqrt{I_*}} \left(1 - \frac{2}{\pi} \right) \gamma_0. \quad (62)$$

The response becomes approximately linear for $\epsilon_2 \ll \beta_2$, or from Eq. (62), when $|\gamma_0| \ll \pi/(2\beta(\pi-2))$. If a standard value of $\beta = \pi$ is considered representative of low \mathcal{R} planforms, the response becomes approximately linear for $|\gamma_0| \ll 25^\circ$. For high \mathcal{R} s with $\beta < \pi$, the linear assumption becomes valid at larger $|\gamma_0|$. Thus the bounding linear solution of Eq. (13) becomes more accurate for high \mathcal{R} s at small $|\gamma_0|$ which is consistent with the yaw response measurements of Barna and Crossman [31] and Hemsch and Luckring [32], who showed that the nonlinear lift decreases with \mathcal{R} .

It is noted that the β_2^2 term neglected in the solution will become evident only in the second approximation of the solution containing ϵ^2 . This justifies neglecting this term in the first approximation of the solution, as stated before.

Another aspect noticed from Fig. 5 is that $\epsilon_2 > \epsilon_1$ and ϵ_1 becomes negative for large values of γ_0 that depend on β . These indicate an increase in damping and a reduction in damped frequency as γ_0 increases. This feature is shown in figure 5(a) of Khedr *et al.* [9], which shows the scaled response measured for two different large values of γ_0 .

A. Truncation error estimation and improved estimate for the frequency

The error in truncating the Chebyshev series at $m = 2$ will increase as the amplitude a reduces as t increases. The error comes mainly from series representation of the $|\sin y|$ terms in (19). The truncation error of the Chebyshev approximation to $|\sin y|$ has a maximum value at $y = 0$ and then decreases exponentially with y , see Rouba *et al.* [33]. The error is also a function of γ_0 as given by the coefficients of the series in terms of ${}_2\tilde{F}_3$ in (46). The error will be higher in $F_1(a)$ in Eq. (50) than in $G_1(a)$ in (51) and consequently will affect the determination of ν at large time. The expression for ν^2 in Eq. (54) has expansion coefficients $a_n = (-1)^n(2n+1) {}_2\tilde{F}_3(2, 1; 5/2, n+5/2, 3/2-n; -\gamma_0^2)$ that converge rapidly as n gets larger so the error can be approximated as $e_n \leq |a_{m+1}|$, Cody [34]. For $m = 2$ the error from Eq. (54) is

$$e_n \leq -\frac{14\beta_1\beta|\gamma_0|\gamma_0}{\sqrt{\pi}} {}_2\tilde{F}_3(2, 1; 5/2, 11/2, -3/2; -\gamma_0^2) \quad (63)$$

This error oscillates $m + 1$ times over the interval $a \in [0, 1]$. For the TCs, e_n will change sign twice but decreases exponentially. e_n was subtracted from ν^2 in Eq. (54) to improve the estimation at large t without significantly compromising the calculations at small t .

V. ANALYTICAL SOLUTION OF YAW RESPONSE

The coefficients $A_k^{(1)}$ and $B_k^{(1)}$ of the differential equations (37, 38) were obtained from Eqs. (35 and 36). Analytical solutions to Eqs. (37, 38) are found in Srivastava and Vishwamittar. [35]. The solution for a in Eq. (37) is

$$a = \frac{a_0 \exp(-\sigma t)}{\sqrt{1 - A_3^{(1)} a_0^2 (1 - \exp(-2\sigma t)) / \sigma - A_5^{(1)} a_0^4 (1 - \exp(-4\sigma t)) / 2\sigma}} \quad (64)$$

Similarly, the solution to ψ in Eq. (38) is

$$\psi = \omega_0 t + B_3^{(1)} K_1 a_0^2 + B_5^{(1)} K_2 a_0^4 + \psi_0. \quad (65)$$

The expressions for K_1 and K_2 are

$$K_1 = -\frac{1}{2\sigma\sqrt{-S}} \quad (66)$$

$$\times \log \left| \frac{S + Q^2 + 2R \left[Q (1 + \exp(2\sigma t)) - \sqrt{-S} (1 - \exp(2\sigma t)) \right] + 4R^2 \exp(2\sigma t)}{S + Q^2 + 2R \left[Q (1 + \exp(2\sigma t)) + \sqrt{-S} (1 - \exp(2\sigma t)) \right] + 4R^2 \exp(2\sigma t)} \right| \quad (67)$$

and

$$K_2 = \frac{1}{2\sigma S} \left[\frac{2P + Q \exp(2\sigma t)}{P + Q \exp(2\sigma t) + R \exp(4\sigma t)} - \frac{2P + Q}{P + Q + R} \right] - \frac{Q}{S} K_1 \quad (68)$$

The coefficients S , Q , and R and P , as given by Srivastava and Vishwamittar. [36], are

$$S = \frac{a_0^4}{\sigma} \left[2\sigma A_5^{(1)} - A_3^{(1)} - 2A_3^{(1)} A_5^{(1)} a_0^2 - A_3^{(1)} a_0^4 \right], \quad (69)$$

$$P = 1 - \frac{A_3^{(1)}}{\sigma} a_0^2 - \frac{A_5^{(1)}}{2\sigma} a_0^4, \quad (70)$$

$$Q = \frac{A_3^{(1)}}{\sigma} a_0^2, \quad (71)$$

and

$$R = \frac{A_5^{(1)}}{2\sigma} a_0^4. \quad (72)$$

The constants a_0 and ψ_0 are determined from the initial conditions as follows:

$$-\dot{\psi}(a_0) a_0 \sin \psi_0 + \dot{a}(a_0) \cos \psi_0 = 0 \quad (73)$$

and

$$\psi_0 = \arccos(1/a_0). \quad (74)$$

For $a_0 \approx 1$ as is usually the case:

$$a_0 = 1 + \frac{1}{2} \left[\frac{A_3^{(1)} + A_5^{(1)} - \sigma}{B_3^{(1)} + B_5^{(1)} + \omega_0} \right]^2. \quad (75)$$

Hence, ψ_0 is determined from Eq. (74).

VI. NUMERICAL VALIDATION OF THE YAW RESPONSE SOLUTION

We now compare the analytical solution of $\gamma = \gamma_0 a \cos \psi$, where a and ψ are given by Eqs. (64) and (65) respectively, to the numerical solution of Eq. (9) without the r_u^2 term as discussed above. Figure 6(a) compares the analytical and numerical solutions for TC1 defined in Subsection II B, with $\gamma_0 = -80^\circ$ and $U = 17$ m/s for which $\epsilon_1 = -0.144$ and $\epsilon_2 = 0.245$ from Eq. (61) when $\beta = 3.45$. (Figure 6(b) is discussed in the last paragraph of this section). The analytic solution is accurate except at large t where the frequency deviates from the numerical calculations. The truncation error either changes sign or becomes much smaller than the value predicted by Eq. (63) for this range. Even when $\epsilon > 1$, however, nonlinear functions that can be expressed as polynomials yield perturbation solutions that converge to their fundamental periodic solution for γ_0^* in Eq. (22). Thus, the method will prevent the error in frequency and damping from transferring to the higher order ϵ terms, Senator and Bapat [37]. The KBM method was shown to provide accurate solutions for $\epsilon = 1$ by, for example, Mendelson [24], using only the fundamental harmonic of the ϵ^0 solution. This means that the deviation in the analytical solution in Fig. 6(a) results mainly from truncating the nonlinear function to allow analytical integration of a and ψ . At the same time, the first order perturbation analysis is sufficient to obtain an accurate solution for TC1 as discussed above and as will be demonstrated further in the next section. Another aspect that was not anticipated when this study began is the *decrease* in the nonlinearity and the series truncation error with increasing $\beta = K_v/K_p$ as discussed in the previous section. The vortex lift results partly from the loss of potential flow due to the suction force resulting from flow separation at the leading edge, which is the basis of the LESA of Polhamus [18]. He gives K_v as

$$K_v = K_p (1 - K_p K_i) / \cos \Lambda \quad (76)$$

where $K_i = \partial C_{Di} / \partial C_l^2$. The induced drag coefficient C_{Di} due to the lift coefficient C_l can be approximated as $K_i \approx 1/(\pi \mathcal{R})$ from potential flow theory. In contrast, the LESA implies the complete loss of leading edge thrust and a fully developed vortex vortex flow which gives $C_{Di}/C_l^2 =$

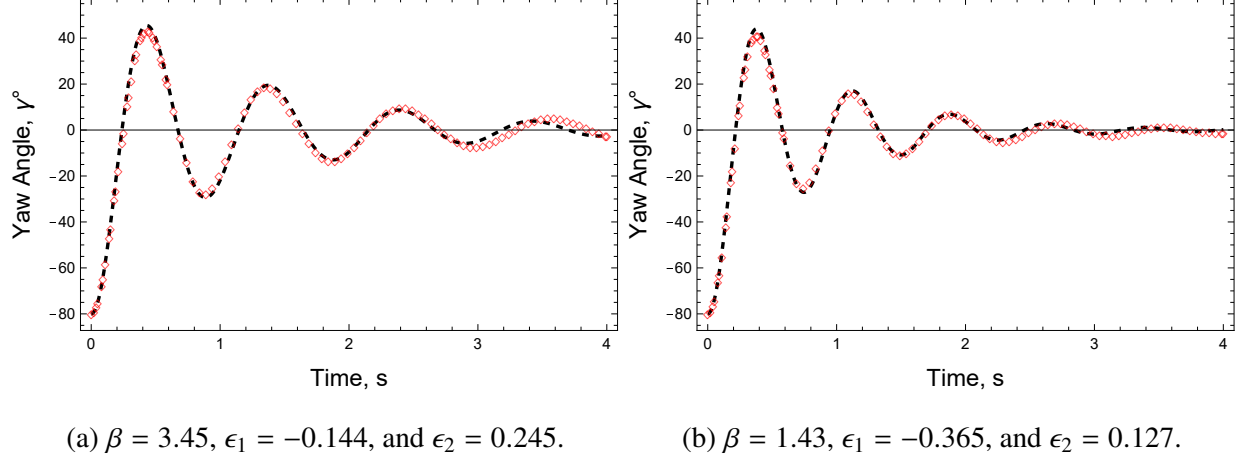


FIG. 6: Results for a) TC1, b) TC2 at $U = 17$ m/s and $\gamma_0 = -80^\circ$ with different $\beta = K_v/K_p$. Numerical solution in red diamonds and analytical solution in black dashed lines.

$\tan \alpha/C_l$, Polhamus [38]. This means that K_v changes significantly with \mathcal{R} as well as with α . Polhamus [18] found that K_v changes very little from the value of π with \mathcal{R} which according to Traub [39] is responsible for inaccurate prediction of C_l using LESA at high \mathcal{R} . Traub [39] derived a simple correlation for K_v that shows a decrease in K_v with \mathcal{R} to asymptote to π as $\mathcal{R} \downarrow 0$. The K_v dependence on α was derived by Purvis [40]. $K_v = 2.36$ was found for delta tail fin of $\mathcal{R} = 1.97$ in Khedr *et al.* [10] using system identification for TC response, a value that is very close to Traub's [2018] correlation. Hence, ϵ will have lower values than given in Fig. 5 as the \mathcal{R} increases as discussed above and in Section IV. In addition, the truncation error will be lower as can be shown by Eq. (63).

Because the experimental implementation of the TC is very straightforward, we believe that the force coefficients, K_p and K_v , are best obtained using system identification as discussed in Khedr *et al.* [10], whereas any change with the γ is dealt with using the separation functions mentioned in Section II and discussed further in Section IX. This is especially the case for the complicated geometries that some small wind turbine manufacturers use for their tail fins, an example of which is described and tested in Khedr *et al.* [10].

Figure 6(b) shows the response of test case TC2 with a delta planform but with $c_0 = 0.143$ m and $b_0 = 0.141$ m, as given in Khedr *et al.* [9]. It has a relatively large $\mathcal{R} = 1.97$, for which the theoretical values of $K_p = 2.184$ and $K_v = \pi$ are used, $r = 0.5383$ m, $I = 0.0376$ kg m², Khedr *et al.* [9], $\gamma_0 = -80^\circ$, and $U = 17$ m/s, giving $I_* = 0.04$ s². $\beta = 1.43$ which is less than half that of TC1. Thus, Eq. (61) gives $\epsilon_1 = -0.365$ and $\epsilon_2 = 0.127$. The comparison with the numerical

solution shows, as expected, that the prediction at large t is better for this higher \mathcal{R} planform.

VII. ACCURATE SOLUTION OF THE MINIMAL EQUATION VIA THE BEECHAM AND TITCHENER METHOD

A more precise solution of the minimal equation can be obtained using the BT method, Beecham and Titchener [2], which avoids the constraints applied in Eq. (26) and the error in expressing the nonlinear functions as truncated polynomials. These advantages of the BT over the KBM method also occur for the equations analysed by Christopher and Thorne [41]. It does not, however, give the amplitude (a) and phase (ψ) in closed form except for the limiting cases.

The restriction used to derive the rate of change of the response in Section III is discussed in detail in Simpson [42]. The restriction is necessary to formulate γ in terms of a and ψ . This is in accordance with the method of variation of parameters and constraints of the form

$$g(a, \zeta, \omega) \cos \psi + h(a, \zeta, \omega) \sin \psi = 0 \quad (77)$$

where g, h are functions of the two variables ζ and ω expressed by Eqs. (28 and 29), respectively. In the KBM the constraints allow formulating $\dot{\gamma}^*$ in a form consistent with the linear response of a second order oscillating system. In this section, however, we use the BT method with its fewer constraints on the definition of $\dot{\gamma}^*$. This results in more accurate, but more complicated, expressions for the a and ψ which do not have closed forms. The BT method, however, provides a compact form of the solution that is better for the analysis of the yaw response.

The BT method uses the two following parameters: $\lambda = \dot{a}_r/a_r$, and the frequency ω_r^2 , so that $\omega_r = \dot{\psi}_r$, where the subscript r is used to distinguish them from those obtained using the KBM method. The two parameters are given in two stage approximations. In the first approximation their definitions are the same as the KBM method but without restriction on the definition of $\dot{\gamma}^*$, and the variables are

$$\lambda_1 = I_1/(2\omega_{r,1}) \quad (78)$$

where the subscript 1 indicates the first approximation. In this approximation, the time rate of change of λ and ω_r in the definition of $\dot{\gamma}_r^*$ are disregarded. Similarly, $\omega_{r,1}$ is given by

$$\omega_{r,1}^2 = \lambda_1^2 + I_2 \quad (79)$$

where I_1 and I_2 are the averages of the nonlinear F function, defined in Eq. (21), over one period of oscillation. They are equivalent to G_1 and F_1 respectively of the KBM method in Eqs. (42 and

41):

$$\begin{aligned} I_1 &= \frac{1}{\pi a_r} \int_0^{2\pi} F(\gamma_r^*, \dot{\gamma}_r^*) \sin \psi_r d\psi_r \\ I_2 &= \frac{1}{\pi a_r} \int_0^{2\pi} F(\gamma_r^*, \dot{\gamma}_r^*) \cos \psi_r d\psi_r \end{aligned} \quad (80)$$

where γ_r^* is defined similarly to KBM method as

$$\gamma_r^* = a_r \cos \psi_r. \quad (81)$$

The assumption used to define $\dot{\gamma}^*$ in Eq. (27) is revised to give

$$\dot{\gamma}_r^* = \lambda_1 a_r \cos \psi_r - \omega_{r,1} a_r \sin \psi_r \quad (82)$$

Then, the first approximations for λ_r and ω_r are used to find more accurate expressions for $\ddot{\gamma}_r^*$ and avoid the assumptions of the first approximation. For the second approximation, Beecham and Titchener [2] give

$$\lambda_2 = \frac{I_1}{2\omega_{r,1} \left[1 + \frac{a_r}{4\omega_{r,1}^2} \frac{d\omega_{r,1}^2}{da_r} \right]} \quad (83)$$

and

$$\omega_{r,2}^2 = \lambda_1^2 + I_2 + \lambda_1 a_r \frac{d\lambda_1}{da_r}. \quad (84)$$

This use of the first approximation to the parameters in the definitions of λ_2 and $\omega_{r,2}$ represents the main assumption of the BT method, Simpson [42]. The consequences of this assumption depends on the particular form of the nonlinear function F ; for the current study we show below that the resulting error is negligible.

The evaluation of I_1 and I_2 in Eq. (80) were obtained using Mathematica. The advantage of the BT method is that no perturbation analysis has to be done after averaging. Thus, the BT method can incorporate the β_2^2 term that is neglected in the KBM solution. The first approximations, again neglecting terms of order β_2^3 and higher as discussed in subsection II A, are

$$I_1 = -\frac{2\beta_2 \omega_{r,1} J_1(\gamma_0 a_r)}{a_r \gamma_0} - \frac{4\beta \beta_2 \cos \mu \operatorname{sign}(\gamma_0) \mathbf{H}_1(\gamma_0 a_r)}{a_r^2 \gamma_0} - \frac{8\beta \beta_2^2 \lambda_1 \omega_{r,1} a_r}{3\pi \beta_1}, \quad (85)$$

and

$$\begin{aligned} I_2 &= \beta_2 \lambda_1 (J_0(\gamma_0 a_r) - J_2(\gamma_0 a_r)) + \frac{\beta_1 J_1(2\gamma_0 a_r)}{a_r} \\ &+ \frac{4\beta \beta_2 \sin \mu \operatorname{sign}(\gamma_0) (a_r \gamma_0 \mathbf{H}_0(\gamma_0 a_r) - \mathbf{H}_1(\gamma_0 a_r))}{a_r^2 \gamma_0} + \frac{\beta \beta_1 \operatorname{sign}(\gamma_0) \mathbf{H}_1(2\gamma_0 a_r)}{a_r} \\ &+ \frac{4\beta \beta_2^2 a_r (2\lambda_1^2 + \omega_{r,1}^2)}{3\pi \beta_1} \end{aligned} \quad (86)$$

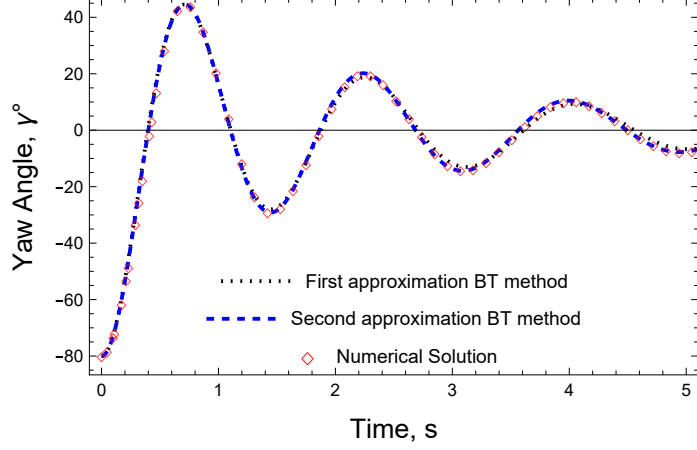


FIG. 7: Results for the BT method for TC1 at $U = 10\text{m/s}$. Numerical solution of Eq. (9) in red diamonds, BT first approximation in dotted black, while second approximation for a delta tail fin released at $\gamma_0 = -80^\circ$.

where $\sin \mu = \lambda_1 a_r$, $\cos \mu = a_r \omega_{r,1}$. This gives λ_1 as

$$\lambda_1 = -\frac{3\pi\beta_1\beta_2 (J_1(\gamma_0 a_r) + 2\beta \text{sign}(\gamma_0) \mathbf{H}_1(\gamma_0 a_r))}{a_r \gamma_0 (4\beta\beta_2^2 a_r + 3\pi\beta_1)}. \quad (87)$$

$\omega_{r,1}$ is obtained from Eq. (79) as

$$\begin{aligned} \omega_{r,1}^2 = & \frac{3\pi\beta_1^2 (J_1(2a_r\gamma_0) + \beta \text{sign}(\gamma_0) \mathbf{H}_1(2a_r\gamma_0))}{a_r (4\beta\beta_2^2 a_r + 3\pi\beta_1)} \\ & + \frac{\beta_1\beta_2^2}{\gamma_0^2 a_r^2 (4\beta\beta_2^2 a_r + 3\pi\beta_1)} \left[3\pi \left(J_1(a_r\gamma_0)^2 - 4\beta^2 \mathbf{H}_1(a_r\gamma_0)^2 \right) \right. \\ & + 8\beta\gamma_0^2 a_r^2 (-J_1(a_r\gamma_0) + J_1(2a_r\gamma_0) - 2\beta \text{sign}(\gamma_0) \mathbf{H}_1(a_r\gamma_0) \\ & + \beta \text{sign}(\gamma_0) \mathbf{H}_1(2a_r\gamma_0)) + 3\pi\gamma_0 a_r (J_1(a_r\gamma_0) + 2\beta \text{sign}(\gamma_0) \mathbf{H}_1(a_r\gamma_0)) \\ & \left. \times (-J_0(a_r\gamma_0) + J_2(a_r\gamma_0) + 4\beta \text{sign}(\gamma_0) \mathbf{H}_2(a_r\gamma_0)) \right]. \end{aligned} \quad (88)$$

The expressions for λ_2 and $\omega_{r,2}$ are too complicated to state here. The Mathematica scripts for their evaluation are available on request from the authors. Nevertheless, both the first and second approximations will be compared against the numerical solution. The response $\gamma^* = a_r \cos \psi_r$ using the first and second approximations are compared in Fig. 7 to the numerical solution of the TC1 for $U = 10 \text{ m/s}$.

The agreement between the first and second BT solutions and the numerical solution is very good. The first approximation shows similar accuracy at high angle and deviates slightly from

both the more accurate second approximation and the numerical solution at large t and small γ . This demonstrates that accuracy of the averaging method; the small deviation of the analytical solution in Fig. 6 comes from the truncation error so the γ_0^* solution in Eq. (23) is sufficient. Also, it shows that approximating $\dot{\gamma}^*$ by Eq. (27) is justified and this demonstrates the validity of the KBM method for the minimal equation.

The accuracy of the first-order approximation and the more compact form of the λ_1 and $\omega_{r,1}$ make them convenient for analyzing the different aspects of the solutions in the following sections. To make the analysis clearer, the neglect of the $O(\beta_2^2)$ terms as done in the KBM method, gives the following simple expressions for λ_1 and $\omega_{r,1}$ with the subscript “1” dropped:

$$\lambda = -\beta_2 [J_1(\gamma_0 a_r) + 2\beta \operatorname{sign}(\gamma_0) \mathbf{H}_1(\gamma_0 a_r)] / (a_r \gamma_0), \quad (89)$$

and

$$\omega_r^2 = \beta_1 [J_1(2a_r \gamma_0) + \beta \operatorname{sign}(\gamma_0) \mathbf{H}_1(2a_r \gamma_0)] / a_r. \quad (90)$$

The expressions are comparable to G_1 and F_1 in Eqs. (44 and 43) respectively. It also shows that the assumption is equivalent to neglecting λ_1^2 from the expression of $\omega_{r,1}$ in Eq. (79).

A. Equivalent linear response

An advantage of the averaging method is the possibility of obtaining a linear system equivalent to the nonlinear one. and so defining the equivalent damping ratio and frequency. Those parameters are valuable in control design and system identification, e.g. Barton *et al.* [43]. The physical interpretation of the “equivalent” system is that both systems have the same energy in a period of oscillation, see Minorsky [44, Ch.14, Sec.7].

An equivalent linear response in the form

$$\ddot{\gamma}_r^* + 2\sigma_e \dot{\gamma}_r^* + \omega_e^2 \gamma_r^* = 0 \quad (91)$$

can be obtained using the above analysis, so that $\sigma_e = -\lambda$ and $\omega_e = \sqrt{\omega_r^2 + \lambda^2} \approx \omega_r$, Beecham and Titchener [2]. To check the validity of the equivalent system, Eq. (91) is solved numerically and compared to the numerical solution of Eq. (19) with the β_2^2 term ignored. Figure 8 shows a satisfactory comparison which demonstrates the accuracy and hence the efficacy of the equivalent linear system. It also validates the approximation $\omega_e \approx \omega_r$. The equivalent system damping ratio,

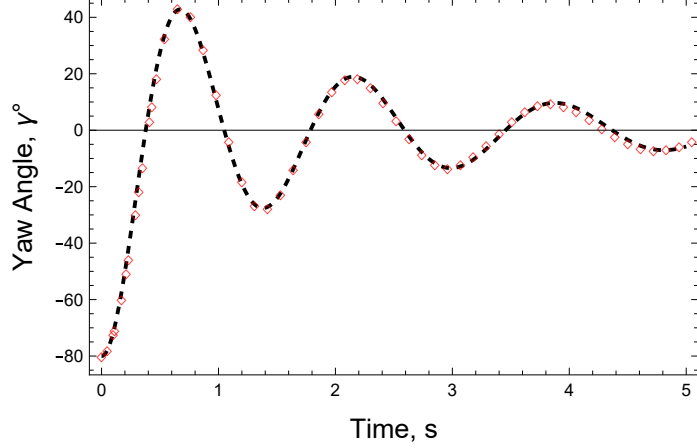


FIG. 8: Equivalent linear solution for TC1 at $U = 10\text{m/s}$. Numerical solution of Eq. (19) in red diamond, equivalent linear solution of Eq. (91) in dashed black of yaw response of a delta fin released at $\gamma_0 = -80^\circ$.

ζ_e , is given by

$$\zeta_e = \frac{\sigma_e}{\omega_e} = \frac{\beta_2}{\sqrt{\beta_1}\gamma_0} \frac{J_1(\gamma_0 a_r) + 2\beta \text{sign}(\gamma_0) \mathbf{H}_1(\gamma_0 a_r)}{\sqrt{a_r (J_1(2\gamma_0 a_r) + \beta \text{sign}(\gamma_0) \mathbf{H}_1(2\gamma_0 a_r))}} \quad (92)$$

B. Logarithmic decrement and response envelope

The logarithmic decrement is a significant parameter in characterising the damping. It is usually linked to linear systems, but when the damping is small, as in the current case, the concept can be used without serious error, Rasmussen [45]. The yaw rate is given exactly by Eq. (82). Setting $\dot{\gamma}^* = 0$ gives the equation for the extrema, γ_p^* , as

$$\gamma_p^* = a_p / \sqrt{1 + (\lambda/\omega_r)^2} = a_p / \sqrt{1 + \zeta_e^2} \approx a_p \quad (93)$$

where a_p is the amplitude at γ_p^* . The relation shows that there is a small phase shift between γ_p^* and the points of coincidence of γ^* and the response envelope. By neglecting the β_2^2 terms of the solution, however, they coincide. The exact relation for the logarithmic decrement, δ , of any cycle i is

$$\delta = \log(a_i/a_{i+1}) \approx \Delta a/a, \quad (94)$$

Panovko and Konyaeva [46]. The approximation is valid for moderate damping where the amplitude changes slowly in one cycle. $\Delta a = T da/dt$ where $T = (2\pi)/\omega_e$ is the period of oscillation.

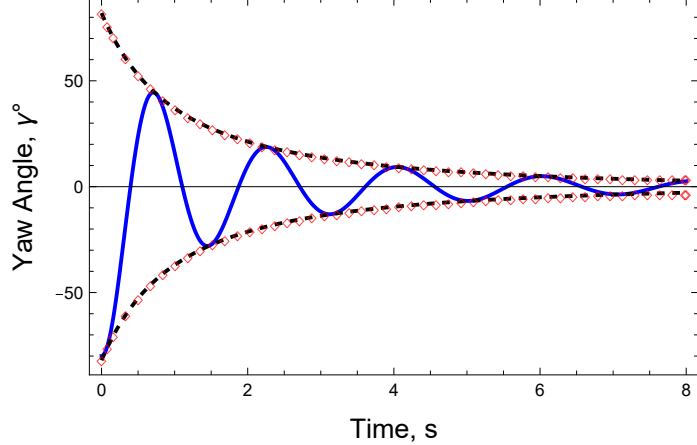


FIG. 9: Response envelope by considering the $\sqrt{1 + \zeta_e^2}$ factor in red diamonds and by disregarding it shown in dashed black for TC1 at $U = 10$ m/s, while the full response is shown in solid blue.

Thus, δ is given by

$$\delta = -2\pi\lambda/\omega_e = 2\pi\zeta_e. \quad (95)$$

For moderate damping, therefore, the logarithmic decrement is equivalent to the damping ratio as in linear systems but is a function of the amplitude. The response envelope from Eq. (93) is plotted in Fig. 9 with a obtained to similar accuracy from either the KBM method, Eq. (64), or by numerically integrating λ from Eq. (89). The figure shows the envelope by considering the factor $\sqrt{1 + \zeta_e^2}$ and by neglecting it. The effect of ζ_e on the response envelope is negligible and Eq. (95) holds with high accuracy.

VIII. BEECHAM AND TITCHENER ANALYSIS AND CORRESPONDING LIMITING MODELS

The BT method has the advantage of providing a compact, accurate expression for the response in terms of the two parameters characterising the nonlinear response, namely λ and ω_r . These parameters include the β_2^2 terms, whereas the KPM method uses the $O(\epsilon^2)$ approximation, given by (87 and 88) for λ and ω_r , respectively. In addition, it was shown in Section IV that ϵ is predominantly linear in γ_0 for an appreciable range of γ_0 . In fact, the actual response is controlled by K_p , K_v , and C_{Dc} at large γ_0 , Khedr *et al.* [9]. The determination of these constants is vital for the successful system identification of any tail fin response, Khedr *et al.* [10]. In this section, therefore, two important limiting cases solutions are developed. We will show that, unexpectedly, K_v enters the

small- $|\gamma|$ response equation.

A. Analytical solution for small yaw angle

An analytical solution for very small $|\gamma_0|$ was derived in Section II C. This second order, linear solution neglects the K_v term in Eq. (4), and was shown to apply for $|\gamma_0| \ll 25^\circ$ for a typical fin in Section IV. This is the basic model used in characterising wind vane response, see for example Barna and Crossman [31] and Kristensen [5]. Barna and Crossman [31], however, found the model failed to predict accurately the damping and frequency of their wind vanes, especially those with low \mathcal{R} , even for $|\gamma_0|$ as low as 5° . In Section IV, this failure was attributed to high values of $\beta = K_v/K_p$ and the consequent increase of nonlinearity. By also using Eq. (10), Khedr *et al.* [10] estimated values of K_p higher than calculated from potential flow theories. In contrast, the solution we now derive by keeping the leading terms of both potential and vortex flow can be used to identify *both* K_p and K_v . In addition, the new solution will extend the upper bound of the linear solution. Only the first order Eqs. (89, 90) are considered. For small $|\gamma_0|$, the leading terms of $J_1(\gamma_0 a_r) \sim (\gamma_0 a_r)/2$, and $\mathbf{H}_1(\gamma_0 a_r) \sim 2(\gamma_0 a_r)^2/(3\pi)$. The equation for a_r becomes

$$\frac{1}{a_r} \frac{da_r}{dt} = -\frac{\beta_2}{2} \left(1 + \frac{8}{3\pi} \beta |\gamma_0| a_r \right) \quad (96)$$

which is easily separated and factored to give

$$a_r = a_{r0} / \left[\exp(\beta_2 t/2) + 8\beta |\gamma_0| a_{r0} (\exp(\beta_2 t/2) - 1) / (3\pi) \right]. \quad (97)$$

where a_{r0} is the value of a_r at $t = 0$. Equation (90) becomes

$$\frac{d\psi_r}{dt} = \omega_r = \sqrt{\beta_1 \gamma_0 (1 + 8\beta |\gamma_0| a_r / (3\pi))}. \quad (98)$$

With the help of Eq. (96), ψ_r is given by

$$\psi_r - \psi_{r0} = -\frac{2\sqrt{\beta_1 \gamma_0}}{\beta_2} \int_{a_{r0}}^{a_r} \frac{da_r}{a_r \sqrt{(1 + 8\beta |\gamma_0| a_r / (3\pi))}}. \quad (99)$$

The solution for the integral, Gradshteyn and Ryzhik [47, No. 2.224.5], is

$$\psi_r = \psi_{r0} + \frac{1}{\zeta_{\text{lin}}} \log \left| \frac{\left(\sqrt{8\beta |\gamma_0| a_r / (3\pi)} + 1 \right) \left(\sqrt{8\beta |\gamma_0| a_{r0} / (3\pi)} - 1 \right)}{\left(\sqrt{8\beta |\gamma_0| a_r / (3\pi)} - 1 \right) \left(\sqrt{8\beta |\gamma_0| a_{r0} / (3\pi)} + 1 \right)} \right| \quad (100)$$

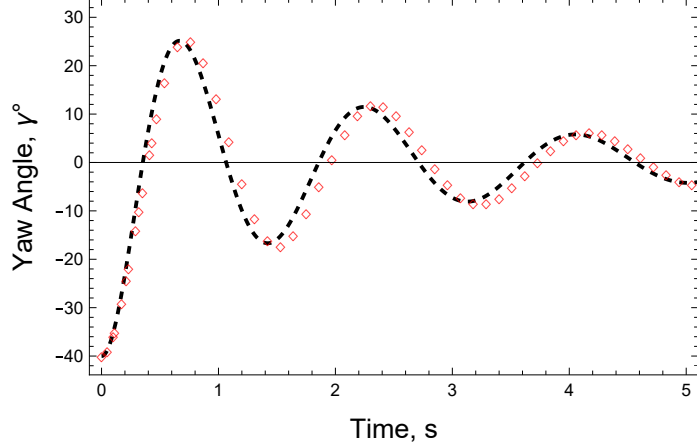


FIG. 10: Results for TC1 at $U = 10$ m/s. Analytical solution of the low γ_0 in dashed black compared to the numerical solution in red diamonds at $\gamma_0 = -40^\circ$.

where $\zeta_{\text{lin}} = \beta_2/(2\sqrt{\beta_1\gamma_0})$, the damping ratio from Eq. (92), is the same as the linear result in Eq. (12), and ψ_{r0} is ψ_r at $t = 0$. The K_v -dependency comes from the logarithmic term. The initial conditions $\gamma_r^*(0) = 1$, $\dot{\gamma}_r^*(0) = 0$ give a_{r0} and ψ_{r0} from Eqs. (81 and 82) as

$$a_{r0} = \left(K^* + \sqrt{K^{*2} + 4(1 + \zeta_{\text{lin}}^2)} \right) / 2 \approx (K^* + 2) / 2 \quad (101)$$

where $K^* = 8\beta|\gamma_0|\zeta_{\text{lin}}^2/(3\pi)$ is also a function of K_v and $a_{r0} = 1$ only in the limit $K_v \downarrow 0$. Further,

$$\psi_{r0} = \arccos(1/a_{r0}). \quad (102)$$

A bound for the validity of this small $|\gamma_0|$ approximation of Eqs. (96 and 100) is set by the $J_1(2\gamma_0)$ approximation in the expression for ω_r in Eq. (90) to give the limit of $J_n(2\gamma_0) \rightarrow \gamma_0$ as $0 < 2\gamma_0 \ll \sqrt{1+n}$, or $|\gamma_0| \ll 180/(\sqrt{2}\pi) \approx 40.5^\circ$. To verify this, this analytical solution is compared with the numerical solution of Eq. (19) for $\gamma_0 = -40^\circ$ in Fig. 10. The comparison is sufficiently satisfactory for the low- $|\gamma_0|$ solution to be accurate for $|\gamma_0| < 40.5^\circ$. The deviation in predicted frequency arises from using the small angle approximation for ω_r in Eq. (90) because it has $2\gamma_0$ as the function argument.

Khedr *et al.* [9] found that the measured response in terms of γ^* changes with $|\gamma_0|$. We again use the subscript “ p ” to denote an extrema, in this case, the subsequent one. Their figure 5 shows results for $\gamma_0 = -80^\circ$. For $|\gamma| \leq \gamma_p = 46.82^\circ$, that is with γ_0 replaced by γ_p and t replaced by $t - t_p$, the data plotted as γ^* were coincident with those for $\gamma_0 = -40^\circ$ where the low- $|\gamma_0|$ approximation should hold. This result provides a formula for the time shift, t_p , from γ_0 to the next γ_p . The

only requirement for collapse is that the amplitude $\gamma_0 a_r$ is the same for the two response or that $a_r \propto \gamma_p / \gamma_0$. From Eq. (97) we have

$$t_p = \frac{2}{\beta_2} \log \left| \frac{a_{r0} |\gamma_0| (1 + 8\beta |\gamma_p| a_{rp} / (3\pi))}{a_{rp} |\gamma_p| (1 + 8\beta |\gamma_0| a_{r0} / (3\pi))} \right| \quad (103)$$

where a_{rp} is the amplitude at γ_p . In the case of Fig. 10, for example, the time to reach the peak $\gamma_{p1} = 25.1^\circ$ calculated using Eq. (103) is 0.69 s which is exact to two decimal places.

Using this analysis it can be shown that if it lies within the validity of the current low- $|\gamma_0|$ model, the response is shifted in time from γ_0 to γ_p . In other words, the response can be considered to restart from γ_p . The frequency and damping must be equivalent according to the equivalent linear system representation of Section VII A. This means that the amplitude is equal to the ratio of the two peaks as stated above and the time shift needed is calculated from Eq. (103). Expanding the normalized angle response $\gamma_r^* = a_r \cos \psi_r$ in the small parameter $g^* = 8\beta |\gamma_0| / (3\pi)$, gives to the first order in g^* :

$$\gamma_r^* = e^{-K_p r_u t_* / 2} \cos \left(\sqrt{K_p} t_* \right) + e^{-K_p r_u t_*} \left(1 - e^{-K_p r_u t_* / 2} \right) \cos \left(\sqrt{K_p} t_* - \phi_g \right) g^* + O(g^{*2}) \quad (104)$$

where the first term on the right is the linear response as given by Eq. (13), and $\tan \phi_g = \sqrt{K_p / I_*} / r_u$ is a constant phase shift. If the first bracketed component of the second term is substituted from Eq. (97), time is shifted by $\approx 2/\beta_2 \log (|\gamma_0| / |\gamma_p|)$, and the amplitude is set to the ratio $a_r = |\gamma_p / \gamma_0|$, then all the γ_0 in Eq. (104) will be replaced by γ_p giving the same response equation but in terms of the angle γ_p . The same holds for the terms of higher orders of g^* as well indicating the equivalence of the responses.

1. System identification of the coefficients K_p and K_v

That the amplitude of motion is proportional to the ratio of the angle extrema has an important application to the use of the low- $|\gamma_0|$ equation for system identification as in Khedr *et al.* [10]. They used Eq. (13) to estimate K_p which ignores the K_v term and thereby overestimated K_p compared to the values taken from the literature. Subsection VIII A showed that at low γ_0 , the extrema of the response can be considered as a new initial condition that is shifted by time t_p from the original one. The test cases TC1 and TC2 are now used to estimate the coefficients K_p and K_v from the low angle section of the original $\gamma_0 \approx -80^\circ$ data, using Eqs. (97, 100, 101, and 102). Taking γ_p now to be any extrema, we arbitrarily chose ones of small magnitude: $\gamma_p = 8.39^\circ$ for TC1 and

-8.75° for TC2. K_v is first optimised and then its definition in terms of K_p given by Eq. (76) was tested where K_i is estimated instead to check the effect of this on overfitting the coefficients. The function “FindFit” in Mathematica was used with its default settings. For TC1, $K_p = 0.9$ and $K_v = 3.11$ were estimated. These are close to the theoretical values $K_p = \pi \mathcal{R}/2 = 0.91$, and $K_v = \pi$ as quoted above and shown in Table II of Khedr *et al.* [9]. For TC2, the estimated values are $K_p = 2.6$ and $K_v = 2.2$; the former is a little higher than the theoretical $K_p = 2.184$ as quoted above from Table II of Khedr *et al.* [9] and the latter is lower than $K_v = \pi$ from the same source. K_v falling below π , however, is consistent with the decrease in K_v with increasing \mathcal{R} as discussed in Section VI and as estimated in Khedr *et al.* [10]. Kohlman and Wentz Jr [48] note that according to Polhamus [18], the LESA overpredicts K_v for large \mathcal{R} delta wings which have insufficient aft surface to generate full vortex lift. Fitting K_v in terms of K_p was found to give the same values of the estimated coefficients for the two test cases. In addition, the results are independent of the initial setting of the coefficients in “FindFit” suggesting a global optimum.

For TC1, $K^* = 0.0031$, $\psi_{r0} = -3.3^\circ$, and the K_v term in Eq. (100) is approximately $1.134t$. For TC2, $K^* = 0.0017$, $\psi_{r0} = -2.4^\circ$, and the K_v term $\approx 1.686t$ which shows the smaller dependency on K_v for high \mathcal{R} tail fins.

Khedr *et al.* [10] also tested and fitted the response of rectangular tail fins. In this case fitting K_v directly using the current model resulted in overpredicted values of K_v compared to those in their study. This is because for rectangular planforms $K_v = K_{v,le} + K_{v,se}$ where “le” and “se” refer to the leading and side edges respectively. The two components have different dependence on K_p resulting in overfitted values. Alternatively, if K_v is found in terms of K_p for the two components using Equations (2, 3, and 4) of Traub [49], $K_p = 0.92$ and $K_v = 3.2$ for the low \mathcal{R} and $K_p = 2.7$ and $K_v = 3.6$ for the high \mathcal{R} one. These values are in very good agreement with the theoretical values in Khedr *et al.* [10] for K_p and the more accurate estimated value of K_v . Using the same procedure to fit the two components of K_v separately, gives, for the low $\mathcal{R} = 0.5$ rectangular fin, $K_{v,le} = 0.8$ and $K_{v,se} = 2.4$, indicating the dominance of the second which asymptotes to π as $\mathcal{R} \rightarrow 0$, DeVoria and Mohseni [50]. This limit contrasts to the value of 2 obtained in Bollay [51].

This discussion and that of Section VI implies that tail fins and wind vanes need different geometries due to their different modes of operation. Tail fins must be effective at high $|\gamma_0|$ to assist turbine starting at low U . Khedr *et al.* [9] note that, once a turbine starts producing power, its tail fin becomes less important for yaw stability. In contrast, wind vanes require excellent linear behavior to minimise $|\gamma|$ at any U . Hence, it is desirable for wind vanes to have high \mathcal{R} whose response

is dominated by the linear K_p term. For tail fins, the delay of stall is important, which requires a low $\mathcal{A}R$ to give a response dominated by the nonlinear K_v term. It is noted that small wind turbines typically have high $\mathcal{A}R$ tail fins; Khedr *et al.* [10] tested a commercial fin with $\mathcal{A}R = 3.71$. Apart from varying the planform, the frequency of the response can be altered through I_* which depends, for example, on the density and thickness of the material comprising the planform and tail boom.

2. Independence of initial conditions and requirements for linearity

Equations (96 and 98) suggest that the low γ_0 solution can become independent of the initial conditions. The β -term for λ and ω_r in Eqs. (89 and 90), respectively, contains the Struve function $\mathbf{H}_n(\gamma_0 a_r)$ which can be expanded as

$$\begin{aligned}\mathbf{H}_n(\gamma_0 a_r) &= \frac{-2\gamma_0^n}{\pi} \sin(\pi\gamma_0) \sum_{k=1}^{\infty} \left[\frac{(-1)^k}{k^2 - \gamma_0^2} \mathbf{H}_n(ka_r) \right] \\ &\sim \frac{-2\gamma_0^n}{\pi} \sin(\pi\gamma_0) \sum_{k=1}^{\infty} \left[\frac{(-1)^k}{k^2} \mathbf{H}_n(ka_r) \right]\end{aligned}\quad (105)$$

Mangulis [52, Part II, Section 10, No. 36], where the approximation is valid for $|\gamma_0| \ll 1$. From Prudnikov and Marichev [53, 6.4.1-3]

$$\csc(\pi\gamma_0) \mathbf{H}_1(\gamma_0 a_r) \sim \frac{2\gamma_0}{3\pi^2} a_r^2 \quad (106)$$

Comparing Eq. (106) to the β -term in (89) gives

$$\frac{1}{a_r} \frac{da_r}{dt} \approx -\frac{\beta_2}{2} \left(1 + \frac{4}{3\pi^2} a_r \right) \quad (107)$$

provided $|\sin(\pi\gamma_0)| \leq 1/(2\beta) \ll 1$. The solution to Eq. (107) can be obtained by replacing $g^* = 8\beta|\gamma_0|/(3\pi)$ in Eqs. (97 and 100) by $4/(3\pi^2)$ and is independent of γ_0 . For TC1 with $\beta = 3.45$, this is valid for $|\gamma_0| \leq 2.6^\circ$ and for $|\gamma_0| \leq 6.5^\circ$ for TC2 with $\beta = 1.43$. This interesting case has been experimentally demonstrated in figure 5(a) of Khedr *et al.* [9] who showed the collapse of normalized responses of TC2 in terms of γ^* for two different release angles of $\gamma_0 = -80^\circ$ and $\gamma_0 = -40^\circ$ only at large t and very low $|\gamma^*|$, indicating independence of γ_0 . This also supports the use of low β for wind vanes to extend the independence to a higher γ_0 , with, however, the penalty of a slower decay rate.

The analysis can be developed further to find the requirements for an exactly linear solution. The following relation holds:

$$\mathbf{H}_1(\gamma_0 a_r) = ((2\gamma_0)/\pi - d(\mathbf{H}_0(\gamma_0 a_r))/d(a_r)) / \gamma_0. \quad (108)$$

From Eq. (105)

$$\mathbf{H}_0(\gamma_0 a_r) = \frac{-2}{\pi} \sin(\pi\gamma_0) \sum_{k=1}^{\infty} \left[\frac{(-1)^k}{k^2 - \gamma_0^2} \mathbf{H}_0(ka_r) \right] \sim \frac{-2}{\pi} \sin(\pi\gamma_0) \sum_{k=1}^{\infty} \left[\frac{(-1)^k}{k^2} \mathbf{H}_0(ka_r) \right]. \quad (109)$$

Prudnikov and Marichev [53, 6.4.1-3] gives the sum of the last series as $-a_r/\pi$. Hence, $\mathbf{H}_1(\gamma_0 a_r) \rightarrow 0$ in Eq. (108) when

$$\sin(\pi\gamma_0) \rightarrow \pi\gamma_0. \quad (110)$$

This makes the solution independent of K_v at sufficiently small values of $\pi|\gamma_0|$ and leads also to $J_1(\gamma_0 a_r) \sim (\gamma_0 a_r)/2$. Using these relations, the solution becomes exactly linear, recovering the linear solution of a_r and ω_r stated in Section III and consequently giving the conditions for the validity of the small $|\gamma_0|$ linear solution in Eq. (13).

We derived in this subsection two important limiting cases of the current model whose validity depends on the magnitude of γ_0 . The first makes the solution independent of β , and exactly linear: $\sin(\pi\gamma_0)/(\pi\gamma_0) \approx 1$. The second makes the solution independent of γ_0 , but with small nonlinearity: $\sin(\pi\gamma_0) \leq 1/(2\beta) \ll 1$. The two limits coincide as $\mathcal{R} \rightarrow 0$, or equivalently $\beta \rightarrow \infty$ where the vortex flow dominates, DeVoria and Mohseni [50]. This condition may have led to the view that yaw response is linear for low \mathcal{R} but becomes nonlinear as \mathcal{R} increases but we have shown that this is true only for $\gamma_0 \rightarrow 0$. We have now reached the unexpected finding that linearity requires the existence of vortex flow only, first for $\beta \rightarrow \infty$ as $|\gamma_0| \rightarrow 0$ and, second, as $\gamma_0 \rightarrow \pi/2$ for $\mathcal{R} \rightarrow \infty$.

B. Analytical solution for large yaw angle

To extend the linear solution from subsection II C, we now derive the nonlinear solution for $|\gamma_0| \gg 1$. The asymptotic expansions of the $J_1(\gamma_0 a_r)$, $\mathbf{H}_1(\gamma_0 a_r)$ from Abramowitz and Stegun [54, §9.2.1, and §9.2.2 and §12.1.31, respectively], are

$$J_1(|\gamma_0| a_r) \sim \sqrt{\frac{2}{\pi |\gamma_0| a_r}} \left[\cos\left(|\gamma_0| a_r - \frac{3\pi}{4}\right) + O\left(\frac{1}{|\gamma_0| a_r}\right) \right] \quad (111)$$

and

$$\mathbf{H}_1(\gamma_0 a_r) \sim \frac{2}{\pi} + \sqrt{\frac{2}{\pi |\gamma_0| a_r}} \left[\sin\left(|\gamma_0| a_r - \frac{3\pi}{4}\right) + O\left(\frac{1}{|\gamma_0| a_r}\right) \right]. \quad (112)$$

Substituting $a_r^* = |\gamma_0|(a_r - 1)$, Eq. (89) becomes

$$\frac{da_r^*}{dt} = -\beta_2 \left[\frac{4}{\pi} \beta + \sqrt{\frac{2}{\pi |\gamma_0|}} \left\{ \left(a_r^* - \frac{a_r^{*2}}{2|\gamma_0|} \right) \cos \delta_a + \left(1 - \frac{a_r^*}{2|\gamma_0|} \right) \sin \delta_a \right\} \right]. \quad (113)$$

where $\delta_a = |\gamma_0| - 3\pi/4 + \phi_a$ and $\phi_a = \arccot(2\beta) \approx 1/(2\beta)$. At small t , a_r varies slowly so $a_r \approx 1$ and all the high order terms of a_r^* can be safely neglected. This reduces the equation to

$$\frac{da_r^*}{dt} = -N_1 a_r^* - M_1. \quad (114)$$

where

$$N_1 = \beta_2 \sqrt{\frac{2}{\pi |\gamma_0|}} \left[\cos \delta_a - \frac{\sin \delta_a}{2|\gamma_0|} \right] \text{ and } M_1 = \beta_2 \left[\frac{4}{\pi} \beta + \sqrt{\frac{2}{\pi |\gamma_0|}} \sin \delta_a \right]. \quad (115)$$

The solution of Eq. (114) is

$$a_r^* = [(M_1 + N_1 a_{r0}^*) \exp(-N_1 t) - M_1] / N_1. \quad (116)$$

So, $a_r = a_r^*/|\gamma_0| + 1$ and $a_{r0}^* = |\gamma_0|(a_{r0} - 1)$.

At very small t , both M_1 and N_1 cancel from Eq. (116) which makes the amplitude linear in t , but the exponential decay quickly becomes important. This means the nonlinearity at high γ_0 results in more rapid decay than a conventional linear system as shown by figure 5(a) of Khedr *et al.* [10]. At high γ_0 , $M_1 \approx 4\beta_2\beta/\pi \propto K_v$. Thus, having a tail fin with high K_v is favourable in general.

At small $|\gamma - \pi/2|$, the K_p -terms are negligible, as stated in Section II C and will be shown in Section IX. This reduces N_1 and M_1 to

$$\begin{aligned} N_1 &= 2\beta\beta_2 \sqrt{\frac{2}{\pi |\gamma_0|}} \left[\cos \left(|\gamma_0| - \frac{3\pi}{4} \right) - \frac{\sin (|\gamma_0| - 3\pi/4)}{2|\gamma_0|} \right], \text{ and} \\ M_1 &= 2\beta\beta_2 \left[\frac{2}{\pi} + \sqrt{\frac{2}{\pi |\gamma_0|}} \sin \left(|\gamma_0| - \frac{3\pi}{4} \right) \right] \end{aligned} \quad (117)$$

Similarly,

$$\psi_r = \psi_{r0} - \frac{1}{N_1} \left[2(\sqrt{z} - \sqrt{z_i}) + \Delta \log \left| \frac{(\sqrt{z} - \sqrt{\Delta})(\sqrt{z_i} + \sqrt{\Delta})}{(\sqrt{z} + \sqrt{\Delta})(\sqrt{z_i} - \sqrt{\Delta})} \right| \right] \quad (118)$$

where $\Delta = M_2 - N_2 M_1 / N_1$, $z = M_2 + N_2 a_r^*$, and $z_i = M_2 + N_2 a_{r0}^*$. N_2 and M_2 are given by

$$\begin{aligned} N_2 &= 2\beta_1 \left[-\frac{\beta}{\pi |\gamma_0|} + \frac{1}{\sqrt{\pi |\gamma_0|}} \left(\cos \delta_b - \frac{3}{4|\gamma_0|} \sin \delta_b \right) \right], \text{ and} \\ M_2 &= \beta_1 \left[\frac{2\beta}{\pi} + \frac{1}{\sqrt{\pi |\gamma_0|}} \sin \delta_b \right] \end{aligned} \quad (119)$$

and $\delta_b = 2|\gamma_0| - 3\pi/4 + \phi_b$ and $\phi_b = \arccot\beta \approx 1/\beta$. Without the K_p - terms:

$$\begin{aligned} N_2 &= 2\beta\beta_1 \left[-\frac{1}{\pi|\gamma_0|} + \frac{1}{\sqrt{\pi|\gamma_0|}} \left(\cos\left(2|\gamma_0| - \frac{3\pi}{4}\right) - \frac{3}{4|\gamma_0|} \sin\left(2|\gamma_0| - \frac{3\pi}{4}\right) \right) \right], \text{ and} \\ M_2 &= \beta\beta_1 \left[\frac{2}{\pi} + \frac{1}{\sqrt{\pi|\gamma_0|}} \sin\left(2|\gamma_0| - \frac{3\pi}{4}\right) \right]. \end{aligned} \quad (120)$$

The initial conditions for the TCs require

$$a_{r0} = \frac{M_1^2}{2(M_2|\gamma_0| - M_1N_1)|\gamma_0|} + 1 \approx \frac{M_1^2}{2(M_2\gamma_0^2)} + 1, \text{ and } \psi_{r0} = \arccos(1/a_{r0}). \quad (121)$$

1. Validation of the high angle solution

The linear solution for $\gamma_0 \rightarrow \pi/2$, Eq. (18), is useful in checking the range of application of the more general equation of the previous subsection. Equation Eq. (18) is accurate when $r_u\dot{\gamma} \ll 1$. At the beginning of motion where the phase angle $\psi_r \approx 0$ and the amplitude $a_r \approx 1$, it can be shown using Eqs. (81, 82) and the definition of λ in Eq. (89) that this term is of the order of $O(\beta_2^2)$ which is considered negligible in the current analysis.

The solution $\gamma = \gamma_0 a_r \cos \psi_r$ can be used for large $|\gamma|$ with a_r and ψ_r taken from Eqs. (116 and 118) respectively. The series expansion of the solution after enforcing the initial conditions and neglecting the $O(\beta_2^2)$ terms reduces to :

$$\gamma = \gamma_0 - \frac{1}{2}M_2\gamma_0 t_*^2 + \frac{1}{24}M_2^2\gamma_0 t_*^4 + O(t_*^6). \quad (122)$$

where t_* is defined in the first paragraph of Section 2.4. The quadratic term $-1/2M_2\gamma_0 t_*^2$ has, from Eq. (120) at $\gamma_0 = \pi/2$, a factor of $3/\pi = 0.955$ compared to the factor of unity in Eq. (18). In order to improve the accuracy of the high- γ solution, the lowest order term omitted from Eqs. (111 and 112) is now added. From Steinig [55], the term is $3\sqrt{2}/(8\sqrt{\pi})(|\gamma_0|a_r)^{3/2} \cos(|\gamma_0|a_r - 3\pi/4)$. The new coefficients of Eqs. (117, 120) are

$$\begin{aligned} N_1 &= 2\beta\beta_2 \sqrt{\frac{2}{\pi|\gamma_0|}} \left[\left(1 - \frac{9}{16\gamma_0^2} \right) \cos\left(|\gamma_0| - \frac{3\pi}{4}\right) - \frac{7}{8|\gamma_0|} \sin\left(|\gamma_0| - \frac{3\pi}{4}\right) \right], \\ M_1 &= 2\beta\beta_2 \left[\frac{2}{\pi} + \sqrt{\frac{2}{\pi|\gamma_0|}} \left\{ \sin\left(|\gamma_0| - \frac{3\pi}{4}\right) + \frac{3}{8|\gamma_0|} \cos\left(|\gamma_0| - \frac{3\pi}{4}\right) \right\} \right] \end{aligned} \quad (123)$$

and

$$\begin{aligned} N_2 &= 2\beta\beta_1 \left[-\frac{1}{\pi|\gamma_0|} + \frac{1}{\sqrt{\pi|\gamma_0|}} \left\{ \left(1 - \frac{15}{64\gamma_0^2} \right) \cos \left(2|\gamma_0| - \frac{3\pi}{4} \right) - \frac{9}{16|\gamma_0|} \sin \left(2|\gamma_0| - \frac{3\pi}{4} \right) \right\} \right] \\ M_2 &= \beta\beta_1 \left[\frac{2}{\pi} + \frac{1}{\sqrt{\pi|\gamma_0|}} \left\{ \sin \left(2|\gamma_0| - \frac{3\pi}{4} \right) + \frac{3}{16|\gamma_0|} \cos \left(2|\gamma_0| - \frac{3\pi}{4} \right) \right\} \right]. \end{aligned} \quad (124)$$

Now the approximation of $H_1(a_r\gamma_0)$ is accurate to $O(|\gamma_0|^{-2})$. For $\gamma_0 = \pi/2$, M_2 has a factor of $3/\pi(1 + 1/(8\pi)) = 0.993$ compared to unity in Eq. (18).

IX. FURTHER DEVELOPMENTS OF THE MINIMAL EQUATION

Two important developments of the minimal equation are discussed here. Neither of them affect the aim of the current study. The first is inclusion of bearing friction. Yaw bearing friction for tail fins was reviewed and studied by Khedr *et al.* [10]. Using system identification, they found that a static friction term, $k_s \operatorname{sign}(\dot{\gamma})$, where k_s is the Coulomb friction coefficient, was the most accurate simple model for their wind tunnel tests. This term, which was also considered by [2], can be simply added to Eq. (4). [2] point out that static friction in the TCs and similar situations should cause the fin to stick at γ_{min} , rather than reach $\gamma = 0$. Then $k_s = K_p|\gamma|_{min}/I_*$ when $|\gamma|_{min}$ is sufficiently small to allow the assumption of Eq. (110) which makes the solution independent of K_v . figure 7 of Khedr *et al.* [9], however, shows the effect of friction at each peak of the response when U has the low value of 5 m/s. Then, both K_p and K_v will contribute to k_s . This confirms the importance of model coefficient identification using wind tunnel tests to describe the interaction between the aerodynamic coefficients and friction constants. Khedr *et al.* [10] found that γ_{min} was either constant or increases with U^{-2} when it presumably depends mainly on the tail fin inertia which influences the yaw loads on the yaw bearings. The ultimate conclusion is that friction will make the damping dependent on U and this would modify the current frictionless model. Fortunately, the solution of the static friction model is straightforward to accommodate within the current solution methods.

The other issue is that Eq. (4) is, in effect, a quasi-steady equation as the only time dependent term in Eq. (1) is generally small. It is known, however, that the force coefficients, K_p and K_v , for fins and vanes are not constant. A simple allowance for their variation is through the separation functions x_i^* s in Eq. (3) which have been used in unsteady aerodynamics modelling for a long time; the most important references for fins and vanes are given in Hammam and Wood [1]. The functions

describe the dynamic process of vortex motion over the fin surface including time lag and separation point movement. These functions are represented as first order differential equations with a time constant $\tau \propto c_0/U$. Because fins and vanes typically have $c_0/x_p \ll 1$, their time scale is very small compared to the time scale of tail fin response $\sqrt{I_*}$. Thus, Hammam and Wood [1] assumed these functions depend only on γ and not on $\dot{\gamma}$, in the simple form of $x_{i,0}^*$:

$$x_i^* \approx x_{i,0}^*(\gamma) = (1 + \exp[\sigma_i(|\gamma| - \alpha_i^*)])^{-1} \quad (125)$$

where σ_i is an empirical constant that expresses the rate of decay of the forcing function and consequently the severity of stall. α_i^* expresses the angle shift in stall characteristics of the tail fin. Khedr *et al.* [9] show that the term in $\dot{\gamma}$ which appears in the full form of Eq. (125) was negligible for their wind tunnel tests.

α_i^* can have different values for each flow component. For potential flow in terms of K_p , it is the stall angle of the tail fin, and for vortex flow in terms of K_v , the α at which the vortex from the tail fin bursts at the apex. At this α , the separation function $x_i^* = 0.5$. Both σ_i and α_i^* are functions of the tail fin sweep angle, or alternatively \mathcal{R} .

These separation functions change the effective K_p and K_v in Eqs. (4 and 9) according to

$$K_p \rightarrow x_{1,0}^* K_p, \quad K_v \rightarrow x_{2,0}^* K_v + (1 - x_{3,0}^*) C_{D,c} \quad (126)$$

where $C_{D,c}$ is the drag coefficient of a normal flat plate which is function also of \mathcal{R} ; Hammam and Wood [1], however, argued that a representative value was 1.3. Thus, the static characteristics of the aerodynamic forces change significantly with yaw angle rather than being described by constant coefficients. For example, the typical value of $K_v = \pi$ is reduced to $C_{D,c} = 1.3$ as $|\gamma| \rightarrow \pi/2$. In addition, $x_{1,0}^* \rightarrow 0$ as $|\gamma| \rightarrow \pi/2$ justifying the neglect of the K_p term in this γ range. This neglect is used to simplify the limiting solutions for $|\gamma_0| = \pi/2$ in Sections II C and VIII B.

A preliminary investigation showed the effect of separation functions on the analytic solution is, as expected, to change of the values of the coefficients K_p and K_v without affecting the form of the solution or its analysis. In practice, an analytical solution including the separation functions is important for accurate prediction of the response compared to experimental measurements, without changing the analysis given here. For that reason, the present study did not include the separation functions.

X. CONCLUSION

The current study describes approximate analytical solutions for the nonlinear yaw response of two important devices; tail fins for aligning small wind turbines with the wind, and wind vanes for measurement of wind direction. Both are thin, swept surfaces that can have any planform and any release angle, γ_0 . The response is given in terms of damped second order differential equation of yaw angle, γ . The model is characterized by two main parameters: $\beta_2 = r/U/\sqrt{I_*}$ and $\beta = K_v/K_p$, where r is the moment arm length, U is the wind velocity, which is assumed constant and coincident with the direction of the longitudinal inertial frame axis, and $\sqrt{I_*}$, the reduced inertia with dimension of s^{-1} . This is the time scale of the current solution. K_v , K_p are, respectively, the vortex flow and potential flow coefficients. Both are strong functions of the aspect ratio, \mathcal{R} , which allows the application of the current models to any planform. Before the present study, the only available analytical solution of the response equation was a second order, linear one involving K_p only. It is restricted to small $|\gamma|$ and low \mathcal{R} . One of the main findings of this study is that K_v influences the response at low $|\gamma|$ and Section 8.1 showed that including K_v in the analysis of wind tunnel results using system identification gave values of K_p and K_v that are more consistent with those in the literature. The literature values were usually determined from steady experiments or calculations, justifying the restriction to a quasi-steady minimal equation of yaw response that is solved in the current study.

Our minimal equation has small nonlinear terms with two perturbation parameters; one for γ while the other for the yaw rate, $\dot{\gamma}$. Both are independent of U but depend mainly on β ; the latter depends also on β_2 . They are linear in γ_0 at low $|\gamma|$ and a function only of K_v while becoming a complicated function of γ_0 at high $|\gamma|$. The small nonlinear damping terms makes the model soluble with a perturbation method. We used the averaging Krylov-Bogoliubov-Mitropolkskii (KBM) method to obtain the amplitude a and phase angle ψ whose time derivative gives the theoretical frequency of the response. An analytical solution is obtained by expanding the nonlinear function in a Chebyshev polynomial which is truncated to give a quintic polynomial of a and approximate closed form solutions are obtained for a and consequently ψ that are valid for any γ_0 . The solution for γ is a function of the model parameters and has a complicated dependence on γ_0 .

The KBM solution is valid for $\beta_2^2 \ll 1$ and found to be accurate compared to a numerical solution, but deviates a little as $|\gamma| \downarrow 0$ and the tail fin settles to equilibrium position at large t . Two test cases are used for the comparison; TC1 with low \mathcal{R} and high β , and TC2 with relatively high

\mathcal{R} but low β . An unexpected finding was that the low β (high \mathcal{R}) causes smaller nonlinearity and lower error from truncating the series used in finding the solution. This is in contrast to the previous linear theories which are linear *because* they are restricted to low \mathcal{R} . High \mathcal{R} gave, therefore, the more accurate response as $|\gamma| \downarrow 0$.

The BT averaging method due to Beecham and Titchener [2] was then used. It is more accurate in that it relaxed the first order approximation of yaw rate used in the KBM method and can accommodate the β_2^2 terms in the solution. Both of those, however, were found to be of marginal importance to the current study as most fins and vanes satisfy $\beta_2^2 \ll 1$ and the KBM approximation to the yaw rate was found to be accurate for $\epsilon < 1$. The BT method, however, provided compact expressions of two important solution parameters: the rate of amplitude decay, $(1/a)da/dt = \lambda$, and rate of change of phase angle, $d\psi/dt = \omega_r$. Neither have an analytical solution over all the γ range except for the limiting cases, $|\gamma| \rightarrow 0$ and $|\gamma| \rightarrow \pi/2$. This large- γ_0 limit was introduced to allow a simple approximate analytic solution, Eq. (18), but the general approximate solutions we derived are valid for any large value of $|\gamma_0| \geq \pi/2$. The limiting cases were used to define an equivalent linear system that has an equivalent damping ratio $\zeta_e = -\lambda/\omega_r$ and an equivalent frequency ω_r . Further, an expression for the logarithmic decrement was obtained in terms of ζ_e .

The compact expressions for λ and ω_r enabled the derivation of closed form analytical solutions for the two limiting cases. For the low $|\gamma_0|$ solution, the amplitude decays at a rate that increases with β . Analysis of the low angle limiting solution shows that the response can restart from any extrema in γ if it is shifted in time from γ_0 and a closed form expression for this time shift is derived. The high angle limiting solution was also derived and validated against the exact analytical solution for $\gamma_0 = \pi/2$. The solution showed that the amplitude decay at very high γ_0 contains a linear and an exponential term indicating the relevance of high K_v for tail fins which can experience high values of $|\gamma|$.

The region of linearity was found in terms of γ_0 to be wherever $\sin(\pi\gamma_0) \approx \pi\gamma_0$. This suggests the use of small \mathcal{R} planforms that have high β for tail fins as the nonlinearity promotes faster response and rapid decay of $|\gamma|$. In contrast, high \mathcal{R} for wind vanes will reduce their nonlinearity. This suggestion is inconsistent with the linear, low- \mathcal{R} theory that is superseded here.

Finally, we note that our approximate analytic solutions to the minimal response equation were derived using the KBM and BT methods in a standard way. Nevertheless, several new mathematical results were required: for the Struve function in Eq. (46), the Bessel function in Eq. (49) in terms of series of an odd Chebyshev polynomial with the former valid only for a positive argument of

the Struve function. Also, section IV contains new series summations of the Weber function, for example, Eq. (61). These may well have general application.

ACKNOWLEDGMENTS

The authors are grateful to Professor Francesco Castellani (Univ. Perugia, Italy) and Dr Amr Khedr (now at EPFL, Switzerland) for their major contributions to the experiments that are cited in the text and used to determine the parameters of the minimal equation. The current study was unfunded. It grew out of a subcontract to the NREL "Distributed Wind Aeroelastic Modeling" program run by Brent Summerville (NREL, USA) to develop the model for a tail fin module for the aeroelastic software OpenFAST. Dr Abhineet Gupta (NREL, USA) was instrumental in this work.

Appendix A: Derivation of the Chebyshev series of $f|f|$

$f = \sin(\gamma_0 \gamma^*) + r_u \gamma_0 \dot{\gamma}^*$, so $f|f|$ is an odd function which when expanded in a Fourier series gives

$$f|f| = -\frac{8}{\pi} \sum_{n=0}^{\infty} \frac{\sin((2n+1)f)}{(2n+1)^3} + 2\pi \sum_{n=0}^{\infty} (-1)^n \frac{\sin((n+1)f)}{(n+1)}. \quad (\text{A1})$$

Let $f = \cos \theta$ and expand the sin terms in a Bessel series as:

$$\begin{aligned} \sin((2n+1) \cos \theta) &= 2 \sum_{m=0}^{\infty} (-1)^m J_{2m+1}(2n+1) \cos((2m+1)\theta) \\ \sin((n+1) \cos \theta) &= 2 \sum_{m=0}^{\infty} (-1)^m J_{2m+1}(n+1) \cos((2m+1)\theta). \end{aligned} \quad (\text{A2})$$

Expressing $f|f|$ in terms of a Chebyshev series as

$$f|f| = \frac{b_0}{2} + \sum_{k=1}^{\infty} b_k T_k(f) \quad (\text{A3})$$

where $f \in [-1, 1]$. The coefficients b_k are determined as

$$b_k = \frac{2}{\pi} \int_0^{\pi} f|f| \cos(k\theta) d\theta. \quad (\text{A4})$$

Substituting Eq. (A2) in (A1) and the result in Eq. (A4), the integral in (A4) is evaluated as

$$\int_0^{\pi} \cos((2m+1)\theta) \cos(k\theta) d\theta = \frac{\pi}{2} \delta_{2m+1,k} \quad (\text{A5})$$

where $\delta_{2m+1,k}$, the Dirac delta function, is zero for $k \neq 2m + 1$. Thus, the Chebyshev series has only odd coefficients given by

$$b_{2k+1} = -\frac{16}{\pi} \sum_{n=0}^{\infty} \frac{J_{2k+1}(2n+1)}{(2n+1)^3} + 4\pi \sum_{n=0}^{\infty} (-1)^n \frac{J_{2k+1}(n+1)}{(n+1)} \quad (\text{A6})$$

and $b_{2k} = 0$. From Prudnikov and Marichev [53] the following series summations are obtained:

$$\begin{aligned} \sum_{n=0}^{\infty} \frac{J_{2k+1}(2n+1)}{(2n+1)^3} &= \frac{\pi^2}{16} \delta_{0,k} + \frac{1}{2(2k+3)(4k^2-1)} \\ \sum_{n=0}^{\infty} (-1)^n \frac{J_{2k+1}(n+1)}{(n+1)} &= - \sum_{n=1}^{\infty} (-1)^n \frac{J_{2k+1}(n)}{n} = 0 \end{aligned} \quad (\text{A7})$$

where the second series summation is valid for $k > 0$. For $k = 0$ the second series gives

$$\sum_{n=1}^{\infty} (-1)^n \frac{J_1(n)}{n} = -\frac{1}{4}. \quad (\text{A8})$$

This remaining term cancels with the $\delta_{0,k}$ term in the summation of the first series of Eq. (A7) resulting in

$$b_{2k+1} = -\frac{8}{\pi} \frac{1}{(4k^2-1)(2k+3)}, \quad (\text{A9})$$

so the Chebyshev series becomes

$$f|f| = -\frac{8}{\pi} \sum_{k=0}^{\infty} (-1)^k \frac{T_{2k+1}(f)}{(4k^2-1)(2k+3)}. \quad (\text{A10})$$

Appendix B: Simplification of the sign function terms in Eq. (9)

The Chebyshev series for the sign term in Eq. (4) is

$$[\sin(\gamma) + r_u \dot{\gamma}]^2 \operatorname{sign} [\sin(\gamma) + r_u \dot{\gamma}] = -\frac{8}{\pi} \sum_{k=0}^{\infty} (-1)^k \frac{T_{2k+1}(\sin \gamma + r_u \dot{\gamma})}{(4k^2-1)(2k+3)} \quad (\text{B1})$$

After expanding T_{2k+1} in a Taylor series to the second order in $r_u \dot{\gamma}$ and some mathematical manipulation using Mathematica, we obtain

$$\begin{aligned} T_{2k+1}(\sin \gamma + r_u \dot{\gamma}) \approx & (-1)^k [\cos((2k+1)\gamma) + (2k+1) \frac{\cos((2k+1)\gamma)}{\cos \gamma} r_u \dot{\gamma} - \\ & \frac{(2k+1)}{2\cos^3 \gamma} ((2k+1) \sin 2k\gamma + 2k \sin \gamma \cos((2k+1)\gamma)) r_u^2 \dot{\gamma}^2] + O(r_u^3 \dot{\gamma}^3) \end{aligned} \quad (\text{B2})$$

Substituting the Chebyshev expansion into Eq. (B1) and summing the series using Mathematica gives the simplified term as

$$[\sin(\gamma) + r_u \dot{\gamma}]^2 \operatorname{sign} [\sin(\gamma) + r_u \dot{\gamma}] \approx \sin \gamma |\sin \gamma| + 2r_u |\sin \gamma| \dot{\gamma} + r_u^2 \dot{\gamma}^2 \operatorname{sign}[\gamma] \quad (\text{B3})$$

to the third order of $O(r_u^3 \dot{\gamma}^3)$, which is used in Eq. (9).

Appendix C: Application of the KBM method

This appendix describes the application of the KBM method as extended by Mendelson [24] for the general case of finite damping in Section III. We assume a periodic solution of Eq. (20) in the phase angle ψ as

$$\gamma^* = \gamma^*(a, \psi). \quad (\text{C1})$$

where the time-dependence of a and ψ are given by:

$$\frac{da}{dt} = \zeta(a), \quad \text{and} \quad \frac{d\psi}{dt} = \omega(a). \quad (\text{C2})$$

γ^* , ζ , and ω are expanded in power of the perturbation parameter ϵ as

$$\begin{aligned} \gamma^* &= \gamma_0^* + \epsilon \gamma_1^* + \epsilon^2 \gamma_2^* + \dots \\ \zeta &= -\sigma a + \epsilon \zeta_1 + \epsilon^2 \zeta_2 + \dots \\ \omega &= \omega_0 + \epsilon \omega_1 + \epsilon^2 \omega_2 + \dots \end{aligned} \quad (\text{C3})$$

The leading terms in the expansions are chosen to give the linear solution of Eq. (20) as $\epsilon \rightarrow 0$.

Substituting the relations in Eq. (C3) into Eq. (20) we obtain

$$\begin{aligned} \omega^2 \frac{\partial^2 \gamma^*}{\partial \psi^2} + & 2\omega \zeta \frac{\partial^2 \gamma^*}{\partial a \partial \psi} + \zeta^2 \frac{\partial^2 \gamma^*}{\partial a^2} + (\zeta \frac{d\omega}{da} + 2\sigma \omega) \frac{\partial \gamma^*}{\partial \psi} + (\zeta \frac{d\zeta}{da} + 2\sigma \zeta) \frac{\partial \gamma^*}{\partial a} + \gamma^* \\ &= \epsilon F \left(\gamma^*, \omega \frac{\partial \gamma^*}{\partial \psi} + \zeta \frac{\partial \gamma^*}{\partial a} \right) \end{aligned} \quad (\text{C4})$$

Equation (C4) to zero order in ϵ is given by

$$\omega_0^2 \frac{\partial^2 \gamma_0^*}{\partial \psi^2} - 2\omega_0 \sigma a \frac{\partial^2 \gamma_0^*}{\partial a \partial \psi} + \sigma^2 a^2 \frac{\partial^2 \gamma_0^*}{\partial a^2} + 2\sigma \omega_0 \frac{\partial \gamma_0^*}{\partial \psi} - \sigma^2 a \frac{\partial \gamma_0^*}{\partial a} + (\omega_0^2 + \sigma^2) \gamma_0^* = 0. \quad (\text{C5})$$

The solution to this equation is

$$\gamma_0^* = a \cos \psi. \quad (\text{C6})$$

Similarly, the first order equation in ϵ is

$$\begin{aligned} \omega_0^2 \frac{\partial^2 \gamma_1^*}{\partial \psi^2} - 2\omega_0 \sigma a \frac{\partial^2 \gamma_1^*}{\partial a \partial \psi} + \sigma^2 a^2 \frac{\partial^2 \gamma_1^*}{\partial a^2} + 2\sigma \omega_0 \frac{\partial \gamma_1^*}{\partial \psi} - \sigma^2 a \frac{\partial \gamma_1^*}{\partial a} + (\omega_0^2 + \sigma^2) \gamma_1^* \\ = 2\omega_0 \omega_1 a \cos \psi + 2\omega_0 \zeta_1 \sin \psi - \sigma a^2 \frac{d\omega_1}{da} \sin \psi + (\sigma a \frac{\zeta_1}{da} - \sigma \zeta_1) \cos \psi \\ + F(a \cos \psi, -\omega_0 a \sin \psi - \sigma a \cos \psi). \end{aligned} \quad (\text{C7})$$

The function F is periodic in ψ as shown by Eq. (32). The terms in $\cos \psi$ and $\sin \psi$ on the RHS of Eq. (C7) must vanish to avoid secular terms in the solution. This condition leads to Eqs. (30 and 31).

Appendix D: Derivation of the Chebyshev series of $|\sin(\gamma_0 \gamma^*)|$

Expanding the even function $|\sin \gamma_0 \gamma^*|$ in a Fourier series gives

$$|\sin(\gamma_0 \gamma^*)| = \frac{2}{\pi} - \frac{4}{\pi} \sum_{n=1}^{\infty} \frac{\cos(2n\gamma_0 \gamma^*)}{4n^2 - 1}. \quad (\text{D1})$$

Let $\gamma^* = \cos \theta$ and substitute the relation from Snyder [22]:

$$\cos(2n\gamma_0 \cos \theta) = J_0(2n\gamma_0) + 2 \sum_{m=1}^{\infty} (-1)^m J_{2m}(2n\gamma_0) \cos(2m\theta). \quad (\text{D2})$$

This gives

$$|\sin(\gamma_0 \cos \theta)| = \frac{2}{\pi} - \frac{4}{\pi} \sum_{n=1}^{\infty} \frac{J_0(2n\gamma_0) + 2 \sum_{m=1}^{\infty} (-1)^m J_{2m}(2n\gamma_0) \cos(2m\theta)}{4n^2 - 1}. \quad (\text{D3})$$

Expressing $|\sin \gamma_0 \gamma^*|$ in terms of Chebyshev series as

$$|\sin(\gamma_0 x)| = \frac{1}{2} b_0 + \sum_{k=1}^{\infty} b_k T_k(\gamma^*) \quad (\text{D4})$$

The series coefficients b_k are determined as

$$b_k = \frac{2}{\pi} \int_0^{\pi} |\sin(\gamma_0 \cos \theta)| \cos(k\theta) d\theta, \quad (\text{D5})$$

or, from Eq.(D3)

$$\begin{aligned} b_k = & \frac{4}{\pi} \int_0^{\pi} \cos(k\theta) d\theta - \\ & \frac{8}{\pi} \int_0^{\pi} \sum_{n=1}^{\infty} \frac{J_0(2n\gamma_0) + 2 \sum_{m=1}^{\infty} (-1)^m J_{2m}(2n\gamma_0) \cos(2m\theta)}{4n^2 - 1} \cos(k\theta) d\theta \end{aligned} \quad (\text{D6})$$

Interchanging the order of summation and integration, the integral gives the coefficients as

$$b_k = \frac{4}{\pi} \left[\delta_{0,k} - 2\delta_{0,k} \sum_{n=1}^{\infty} \frac{J_0(2n\gamma_0)}{4n^2 - 1} \right] - \frac{8}{\pi} \sum_{k=1}^{\infty} (-1)^k \left[\sum_{n=1}^{\infty} \frac{J_{2k}(2n\gamma_0)}{4n^2 - 1} \right] \quad (\text{D7})$$

where

$$b_0 = \frac{4}{\pi} \left[1 - 2 \sum_{n=1}^{\infty} \frac{J_0(2n\gamma_0)}{4n^2 - 1} \right]. \quad (\text{D8})$$

Substituting Eqs. (D8 and D7) into (D4) and summing the series in (D7) gives

$$\sum_{n=1}^{\infty} \frac{J_{2k}(2n|\gamma_0|)}{4n^2 - 1} = \frac{1}{4} [2\delta_{0,k} + \pi E_{2k}(|\gamma_0|)] \quad (\text{D9})$$

where δ is the Dirac delta function which is zero for $k \neq 0$, e.g. [53]. Substituting $k = 0$ in Eq. (D9) gives

$$\sum_{n=1}^{\infty} \frac{J_0(2n|\gamma_0|)}{4n^2 - 1} = \frac{1}{4} [2 + \pi E_0(|\gamma_0|)]. \quad (\text{D10})$$

[1] M. M. Hammam and D. Wood, *Modeling the Yaw Behavior of Tail Fins for Small Wind Turbines*, Technical Report NREL-86044 (NREL, 2023).

[2] L. Beecham and I. Titchener, *Some Free Notes on an Approximate Oscillation Characteristics of Systems Typified by $\ddot{x} + F(x, \dot{x}) = 0$* , Technical Report 3659 (ARC Reports and Memorandum, 1969).

[3] D. Wood, *Small Wind Turbines: Analysis, Design, and Application* (Springer, 2011).

[4] D. R. Bradney, S. P. Evans, M. S. P. D. Costa, and P. D. Clausen, Comparison of computational modelling and field testing of a small wind turbine operating in unsteady flows, in *Journal of Physics: Conference Series*, Vol. 753 (IOP Publishing, 2016) p. 082029.

[5] L. Kristensen, *Cups, props and vanes*, Technical Report R-766 (Risø National Laboratory., 1994).

[6] T. S. Hristov, S. D. Miller, and C. A. Friehe, Linear time-invariant compensation of cup anemometer and vane inertia, *Boundary-layer Meteorology*. **97**, 293 (2000).

[7] H. Kerhascoët, J. Laurent, A. Cerqueus, M. Sevaux, E. Senn, F. Hauville, and R. Coneau, Methodology for optimal wind vane design, in *OCEANS 2016-Shanghai* (IEEE, 2016) pp. 1–7.

[8] K. Singh, A. Hemmati, and D. H. Wood, The aerodynamic characterization of generic tail fin shapes, *Wind Engineering*. **63**, 493 (2012).

[9] A. A. Khedr, M. M. Hammam, A. Gupta, E. Branlard, F. Castellani, and D. H. Wood, The nonlinear behaviour of generic tail fins for small wind turbines, *Journal of Renewable and Sustainable Energy*. **16** (2024).

[10] A. A. Khedr, M. M. Hammam, A. Gupta, F. Castellani, and D. H. Wood, Using system identification in modelling the yaw response of tail fins for small wind turbines with bearing friction, *Journal of Renewable and Sustainable Energy*. **17** (2025).

[11] M. M. Hammam and D. H. Wood, Aeroelastic modelling of tail fins for small wind turbines, in *Journal of Physics: Conference Series*, Vol. 2265 (IOP Publishing, 2022) p. 042073.

[12] R. E. Mickens, *An Introduction to Nonlinear Oscillations* (Cambridge University Press., 1981).

[13] N. N. Krylov and N. Bogoliubov, *Introduction to Non-linear Mechanics* (Princeton University Press., 1947).

[14] N. N. Bogoliubov and Y. A. Mitropolskii, *Methods in the Theory of Nonlinear Oscillations* (CRC Press., 1961).

[15] J. Wieringa, Evaluation and design of wind vanes, *Journal of Applied Meteorology and Climatology*. **6**, 1114 (1967).

[16] H. H. Jonsson, Response characteristics of an oscillatory vane for flow-speed measurements, *Journal of Applied Physics*. **64**, 6175 (1988).

[17] A. Robinson and J. A. Laurmann, *Wing Theory* (Cambridge University Press., 1956).

[18] E. C. Polhamus, *A concept of the vortex lift of sharp-edge delta wings based on a leading-edge-suction analogy*, Technical Report TN-D-3767. (NASA, 1966).

[19] J. M. Luckring, Selected scientific and technical contributions of edward c. polhamus, in *34th AIAA Applied Aerodynamics Conference* (AIAA, 2016) p. 3565.

[20] P. R. Ebert and D. H. Wood, On the dynamics of tail fins and wind vanes, *Journal of Wind Engineering and Industrial Aerodynamics*. **56**, 137 (1995).

[21] J. E. Lamar, *Extension of leading-edge-suction analogy to wings with separated flow around the side edges at subsonic speeds*, Technical Report L-9460 (NASA, 1974).

[22] M. A. Snyder, *Chebyshev methods in numerical approximation* (Prentice-Hall., 1966).

[23] F. W. J. Olver, A. B. O. Daalhuis, D. W. Lozier, B. I. Schneider, R. F. Boisvert, C. W. Clark, B. R. Miller, B. V. Saunders, H. S. Cohl, and M. A. McClain, *NIST Digital Library of Mathematical Functions* (<https://dlmf.nist.gov/>, Release 1.2.4 of 2025-03-15, 2025).

[24] K. S. Mendelson, Perturbation theory for damped nonlinear oscillations, *Journal of Mathematical Physics*. **11**, 3413 (1970).

[25] G. N. Bojadziev, Damped oscillating processes in biological and biochemical systems, *Bulletin of Mathematical Biology* **42**, 701 (1980).

[26] A. Beléndez, D. I. Méndez, E. Fernández, and S. Marini, An explicit approximate solution to the duffing-harmonic oscillator by a cubication method, *Physics Letters A* **373**, 2805 (2009).

[27] A. C. Teron, A. Bartlett, N. Duan, and K. Sun, Estimating the nonlinear oscillation frequency of a power system using the harmonic balanced method, in *2016 IEEE Power and Energy Society General Meeting (PESGM)* (IEEE, 2016) pp. 1–5.

[28] A. Actor, More on zeta-function regularization of high-temperature expansions, *Fortschritte der Physik/Progress of Physics* **35**, 793 (1987).

[29] Y. Luke, *The Special Functions and Their Approximations, vol. 1* (Academic Press., 1969).

[30] J. C. Straton, ${}_3F_4$ hypergeometric functions as a sum of a product of ${}_2F_3$ functions, *Axioms* **13**, 203 (2024).

[31] P. S. Barna and G. R. Crossman, *Experimental studies on the aerodynamic performance and dynamic response of flow direction sensing vanes*, Technical Report 75-T7 (NASA, 1976).

[32] M. J. Hemsch and J. M. Luckring, Connection between leading-edge sweep, vortex lift, and vortex strength for delta wings, *Journal of Aircraft* **27**, 473 (1990).

[33] Y. Rouba, P. Patseika, and K. Smatytski, On a system of rational chebyshev–markov fractions, *Analysis Mathematica* **44**, 115 (1993).

[34] W. Cody, A survey of practical rational and polynomial approximation of functions, *Siam Review* **12**, 400 (1970).

[35] S. Srivastava and Vishwamittar., Application of perturbation theory to the damped sextic oscillator, *Journal of Mathematical Physics* **30**, 2815 (1989).

[36] S. Srivastava and Vishwamittar., Erratum: Application of perturbation theory to the damped sextic oscillator, *Journal of Mathematical Physics* **32**, 564 (1991).

[37] M. Senator and C. N. Bapat, A perturbation technique that works even when the non-linearity is not small, *Journal of Sound and Vibration* **164**, 1 (1993).

[38] E. C. Polhamus, Predictions of vortex-lift characteristics by a leading-edge suction analogy, *Journal of aircraft* **8**, 193 (1971).

[39] L. W. Traub, Extending the leading-edge suction analogy to nonslender delta wings, *Journal of Aircraft* **55**, 2176 (2018).

[40] J. W. Purvis, Analytical prediction of vortex lift, *Journal of aircraft* **18**, 225 (1981).

[41] P. A. T. Christopher and R. Thorne, Some examples of the application of the beecham-titchener-simpson (bts) method to autonomous systems, *The Aeronautical Journal* **89**, 380 (1985).

[42] A. Simpson, An algorithm for autonomous non-linear dynamical equations, *Aeronautical Quarterly.* **164**, 211 (1977).

[43] R. L. Barton, D. Olsen, and B. Redd, *Relationship between the aerodynamic damping derivatives measured as a function of instantaneous angular displacement and the aerodynamic damping derivatives measured as a function of oscillation amplitude*, Technical Report TN-D-2855 (NASA, 1965).

[44] N. Minorsky, *Nonlinear Oscillations* (Van Nostrand Co., Inc., Princeton, N. J., 1962).

[45] M. L. Rasmussen, On the damping decrement for non-linear oscillations, *International Journal of Non-Linear Mechanics.* **12**, 81 (1977).

[46] Y. Panovko and M. Konyaeva, *Elements of the applied theory of elastic vibration* (MIR, Moscow., 1971).

[47] I. S. Gradshteyn and I. M. Ryzhik, *Table of Integrals, Series, and Products* (Academic Press., 2014).

[48] D. L. Kohlman and W. H. Wentz Jr, *Wind tunnel investigations of vortex breakdown on slender sharp edged wings Final report*, Technical Report CR-98737 (NASA, 1968).

[49] L. W. Traub, Examination and prediction of the lift components of low aspect ratio rectangular flat plate wings, *Aerospace MDPI.* **10**, 597 (2023).

[50] C. DeVoria, A and K. Mohseni, A vortex model for forces and moments on low-aspect-ratio wings in side-slip with experimental validation, *Proc, Royal Soc. A* **473**, 20160760 (2017).

[51] W. Bollay, A non-linear wing theory and its application to rectangular wings of small aspect ratio, *ZAMM-Journal of Applied Mathematics and Mechanics.* **19**, 21 (1939).

[52] V. Mangulis, *Handbook of Series for Scientists and Engineers* (Elsevier., 2012).

[53] A. P. Prudnikov and O. I. Marichev, *Integrals and series: special functions (Vol. 2)* (CRC press., 1966).

[54] M. Abramowitz and I. A. Stegun, *Handbook of Mathematical Functions: with formulas, graphs, and mathematical tables* (Dover, New York., 1972).

[55] J. Steinig, The real zeros of struve's function, *SIAM Journal on Mathematical Analysis.* **1**, 365 (1970).